FRONT MATTER

Title

- Full title: **Mapping the potential risk of coronavirus spillovers in South and Southeast Asia**
- Short title: **Mapping potential coronavirus spillover risk in Asia**

Authors

Ralph Sedricke Lapuz[1], Ada Chornelia[1], Alice C. Hughes[1,2,*]

Affiliations

[1] School of Biological Sciences, The University of Hong Kong, Pokfulam Road, Hong Kong SAR, China

[2] School of BioSciences, Faculty of Science, The University of Melbourne, Biosciences 4, The University of Melbourne, Royal Parade, Parkville VIC 3010, Australia

*Corresponding author email: achughes@hku.hk; alice.c.hughes@unimelb.edu.au

Abstract

Bats harbor approximately a third of known mammal viruses, including recent coronaviruses that caused pandemics. As spillover risk increases due to habitat loss and fragmentation, utilizing a OneHealth approach, we identified potential zoonotic spillover and pandemic risk hotspots in South and Southeast Asia. We used a model that estimates the risk of infectious disease emergence by incorporating Rhinolophid bat species distribution, forest fragmentation, and human population density data. Results showed that spillover risk hotspots are concentrated in Indochina and southern China, where species richness and fragmentation are high, and where coronaviruses were previously detected in bat populations. Simulation of pandemic spread from the spillover risk hotspots using network models revealed risk hotspots clustered in Bangladesh and northeast India. These results highlight the regional vulnerability of human population centers and heightened risks from habitat fragmentation. Our work emphasizes a multidisciplinary approach to safeguard public health and ecosystems by identifying hotspots, advocating for mitigation measures, and enhancing surveillance in vulnerable regions.

Teaser

Bats in Asia pose pandemic risks due to hosting coronaviruses. We used a OneHealth approach to map risk hotspots for emerging diseases.

MAIN TEXT

Introduction

An estimated 60-75% of emerging infectious diseases for humans originate from zoonotic pathogens coming from wildlife (*1*, *2*). Various taxa may be particularly likely to host zoonotic pathogens, with rodents, bats, and to some extent, carnivores well known for their capacity to host and transmit pathogens (*3–6*). With increasing habitat loss and degradation, climate change, and exposure to various chemicals, zoonotic spillovers from wildlife may increase into the future, yet these patterns and risks depend on the hosts (*7–9*). The probability of spillover relates to changes in two interrelated factors: firstly, changes in the interface between different animals, which alters the potential for wildlife to contract or spread pathogens, and secondly, stressors which may alter the vulnerability of animals to become sick or alter the rate of viral shedding (*10*, *11*). Habitat loss and fragmentation do both, as they increase potential interfaces for spillover, as increasing these interfaces both surge the opportunity for potential competent hosts to meet (and exchange pathogens) and increases the stress level of wild animals, which may increase susceptibility to infection (*12*). Understanding the potential for spillover requires knowing the interfaces where wildlife interacts with humans, livestock, and domestic animals, including how these connect to human population centers. Competent hosts are frequently commensal with humans, thus as areas are destroyed and degraded the probability of wild species harboring and spreading pathogens increases (*13–15*).

Bats represent a prominent group of competent hosts, which harbor a significantly higher percentage of zoonotic viruses compared to other mammals (*4*). This ability to host diverse viruses, often without showing symptoms, is likely due to the high metabolic costs (and associated ecophysiological pressures) associated with flight (*16–18*). Consequently, several pathogens which infect bats originally continue to impact human populations in recent decades (*11*, *19*, *20*). Fruit bats (Pteropodidae) are reservoirs of Hendra virus (Australia, 1994), Nipah virus (Malaysia, 1998-99), Marburg virus (Central Africa), and possibly Ebola virus (Central-Western Africa). Yet different viruses have different hosts, and horseshoe (Rhinolophidae) bats provide reservoirs of beta-coronaviruses (*21*, *22*) including SARS-CoV1 in 2003, SARS-CoV2 in the COVID-19 pandemic in 2019, and the MERS-CoV outbreak in the Middle East in 2012 (*23*, *24*). Rhinolophid species richness peaks in tropical east Asia (*25*), and given the distribution of previous betacoronavirus pandemic outbreaks, it is a key region for further work to understand the risk of potential future spillover events. In previous outbreaks, the viruses are thought to have spilled over

from bats to an intermediate host (e.g. horses for Hendra, pigs for Nipah, palm civets for SARS) that is closely associated with humans (*11*). Thus, understanding how landscape structure interfaces with species distributions, especially those of competent hosts for any given pathogen, may provide insights into where and even when the probability of spillover may occur. For example, in the case of Hendra, the loss of habitat due to deforestation coupled with periods of winter drought forced *Pteropus alecto* into horse pastures to forage, and this increase in stress in conjunction with increased interface with horses is specifically associated with spillover events (*19*). In South and Southeast Asia, higher spillover risk of Nipah virus from *Pteropus* fruit bats was predicted in areas with greater human footprint (*26*), specifically in regions with higher human settlements and livestock or food sources for the bats (*27*). Yet our understanding of these interacting elements of risk are limited to a few examples, despite the critical role of bats as sources of a diverse variety of zoonoses.

A OneHealth approach emphasizes the interconnectedness of human, animal, and environmental health (*28*, *29*). The use of this approach in detecting potential spillover risk in connection to ecological imbalances arising from human impacts on the environment has been increasing in the past decade (*1*, *8*, *9*, *19*, *30*). Regions such as Southeast and South Asia may be at particular risk due to the high rates of habitat loss coupled with high diversity, and high human population densities (*1*, *4*, *30–32*). Furthermore, whilst studies have attempted to explore the risk of spillover from Southeast Asia, limited data on both habitat quality and species diversity may hamper the accuracy of such approaches (*33*).

In this study, we assess the potential risk of betacoronavirus spillover arising from their most frequent reservoir host, the horseshoe bats (*Rhinolophus*), in tropical east Asia using a OneHealth approach. We also explored potential pandemic spread scenarios given planned infrastructure in the region. This is crucial since a developing region with planned infrastructure may negatively impact wildlife in sensitive habitats (*34*) and create new interfaces for zoonotic spillover. Investigating locations of potential hotspots in Asia provides insights into the dynamics of virus emergence, allowing targeted action to counteract those risks.

Results

Mapping potential spillover risk hotspots

Based on relative estimated risk of disease emergence (eRIDE) indices computed across the whole region, the majority of the potential spillover risk hotspots are concentrated in China and Indochina (Myanmar, Laos, Vietnam, Cambodia and Thailand), which collectively account for almost three-quarters (74.1%) of the total relative eRIDE (Figures 1a and 2a; Table S4). The highest risk areas are in the montane and forested regions of the countries of Indochina. Concerning individual country risks, Laos and Vietnam have over half of their land areas categorized as the highest eRIDE risk, at 56.5% and 51.3%, respectively (Figure 3; Table S5). For China, 12.0% of its area is classified as the highest eRIDE risk, with most found in its southern areas adjacent to Indochina. India has 7.4% of its area classified as the highest eRIDE risk, and 42.5% of its land area is at moderately high eRIDE risk, particularly in its northeast region and the Western Ghats. In Bangladesh, 7.4% of its area is at highest eRIDE risk, while 70.9% of its land area is classified as moderately high risk. In the insular region, Indonesia has 10.8% of its land area categorized as moderately high eRIDE risk, concentrated in Sumatra and Kalimantan (Borneo), followed by Sulawesi and Papua (Figure 3; Table S5).

The spatial distribution of population-at-risk (PAR) indices resembles that of eRIDE, suggesting that the populations at risk are near the spillover risk hotspots (Figure 1). These hotspots are spatially concentrated in Nepal, northeast India, western Myanmar, Vietnam, and southern China (Figure 1b). Countries with the highest relative PAR scores (computed for across the entire region) are those with the largest populations. China registered the highest relative PAR score (29.6%), followed by India (21.2%), and Indonesia (13.5%) (Figure 2b; Table S4). Concerning individual country risks, Singapore recorded 86.1% of its population at the highest risk, followed by Sri Lanka (82.2%), Vietnam (76.0%), and Bangladesh (75.1%) (Figure 3; Table S6). Notably, India and China registered 46.5% and 36.5% of their large populations at the highest risk, respectively.

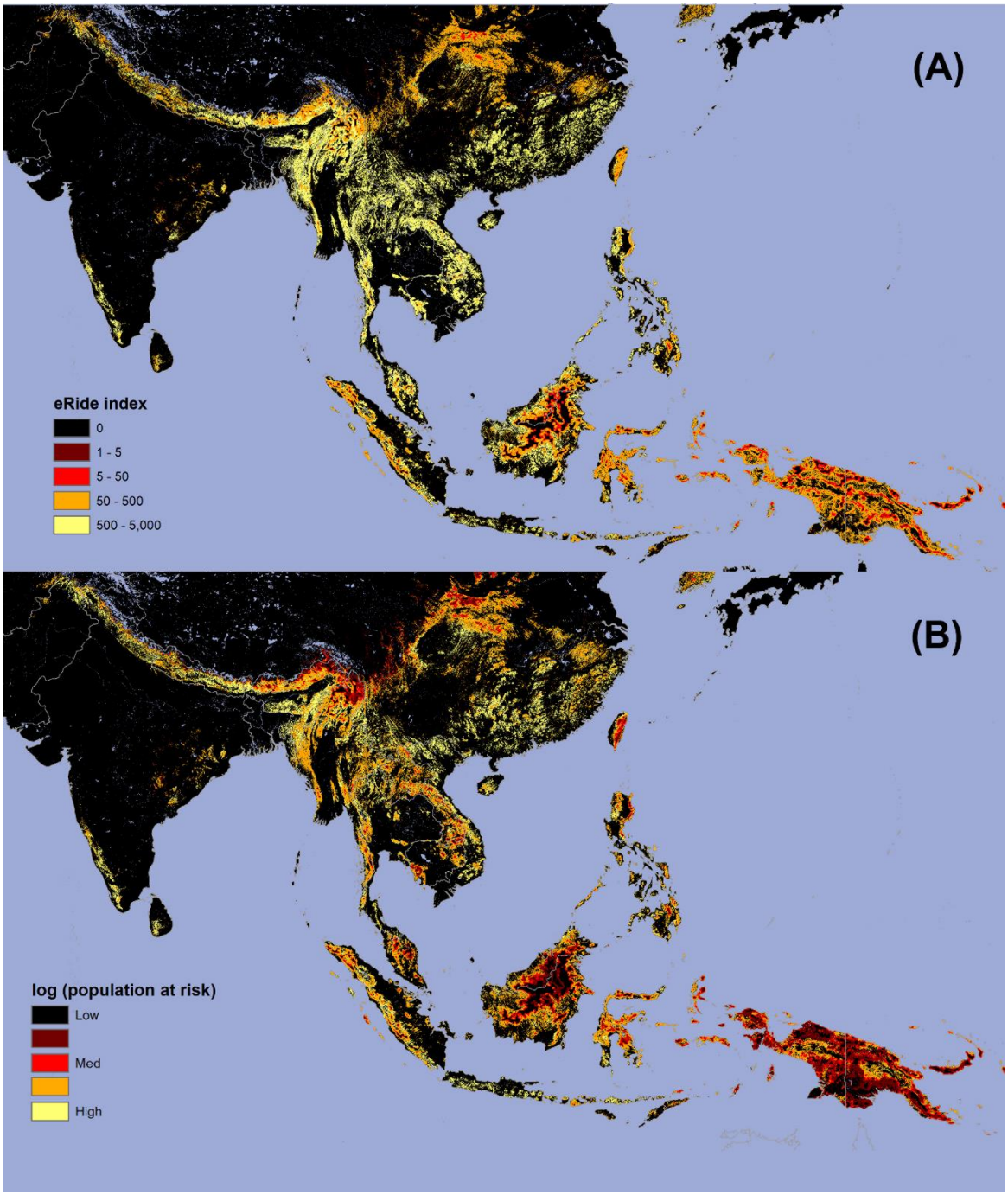

Figure 1. Zoonotic Risk Hotspots in Rhinolophid Bats of Tropical East Asia. Maps of tropical East Asia showing risk hotspots from zoonotic agents in Rhinolophid bats of tropical East Asia. Depicted here are (**A**) eRIDE and (**B**) Population at risk (PAR, log values displayed for clarity) scores. For both maps, discrete color bands follow a geometric scale.

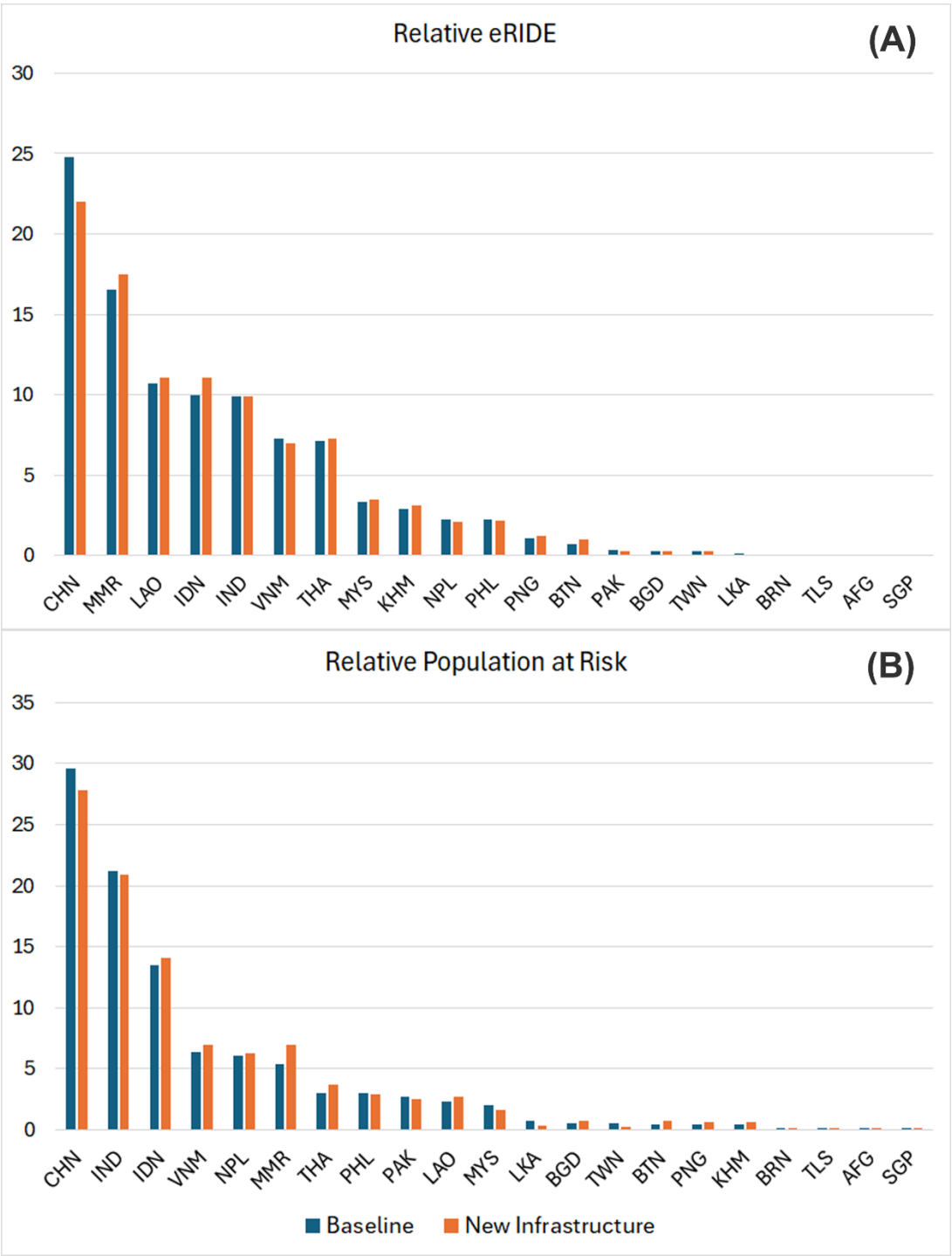

Figure 2. Index rankings per country under baseline (blue) and new infrastructure (orange) scenarios. Numbers displayed are the sums of all (**A**) eRIDE index and (**B**) PAR values within each country's boundaries as shown in Figure 1. Decreases are due to losses of small fragments due to the resolution of analysis.

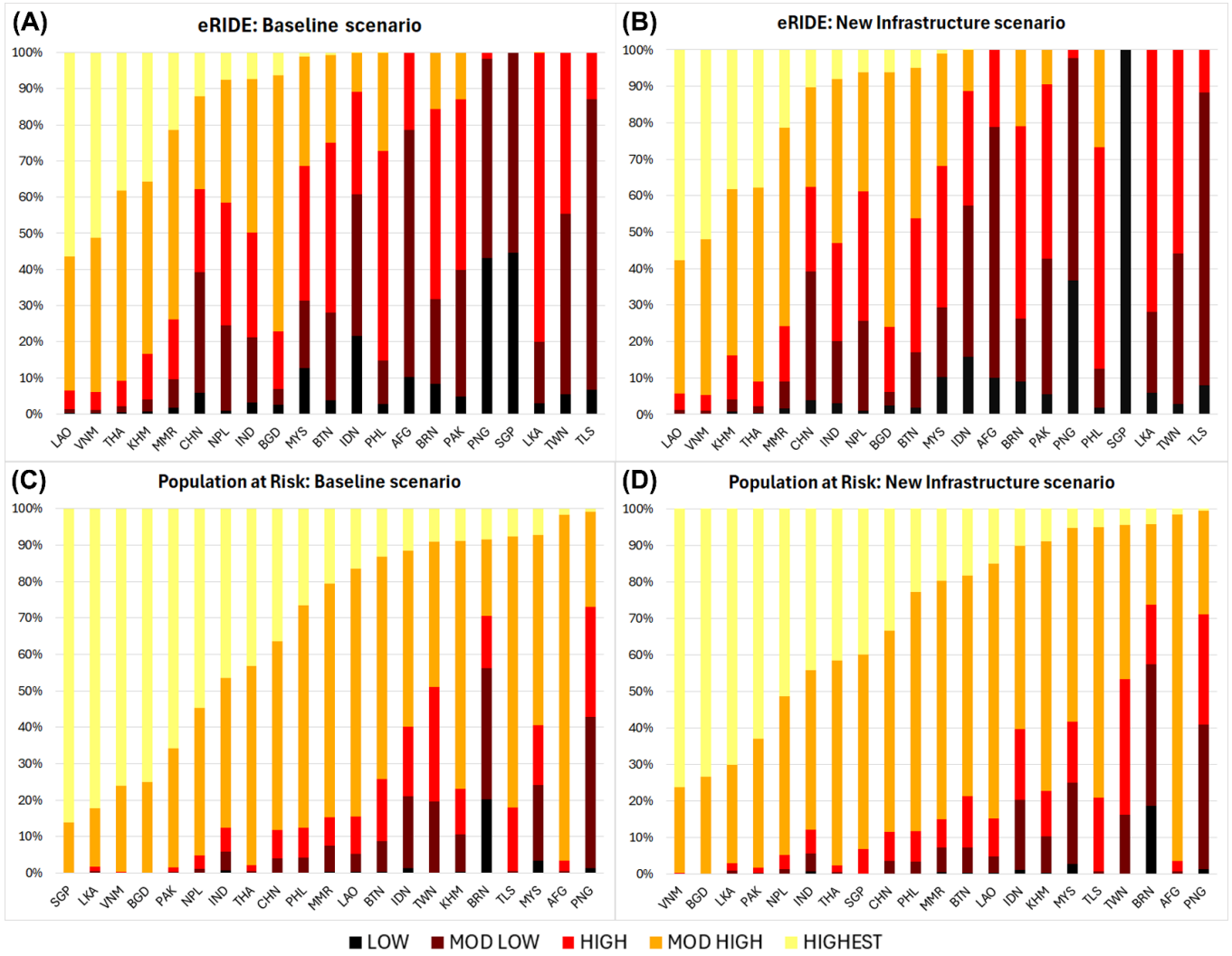

Figure 3. Country Risk Class Distributions: Baseline vs. New Infrastructure Scenarios. Stacked bar plots illustrating the distribution of risk classes per country in tropical East Asia, categorized by eRIDE and Population at Risk scores for baseline (**A, C**) and new infrastructure (**B, D**) scenarios. The color scheme denotes varying risk levels, with yellow indicating the highest risk category and black representing the lowest risk category.

Pandemic risk mapping

Pandemic spread modeling showed that the countries with highest pandemic risk are China, Bangladesh, and India (Figure 4). Specific areas in South Asia where pandemic risk is highest are in the majority of Bangladesh, India's north, northeast, and southern regions, and eastern Pakistan (Figure 4a). India and China have the highest relative pandemic risk scores, respectively garnering 47% and 30% out of a total possible 100% computed for the entire region (Figure 4b; Table S4). They are followed to a lesser extent by Bangladesh (5.5%) and Pakistan (5.4%), although they are notably smaller in terms of size than the previous two countries. In China, the surrounding coastal areas of the large Chinese cities of the Greater Bay Area (Guangzhou, Shenzhen, Hong Kong and Macau) and Shanghai are the highest pandemic risk areas. Pockets of high-risk areas also exist in cities in Myanmar, Thailand, Indonesia, Vietnam, Malaysia, and the Philippines.

Among all countries, Bangladesh recorded the largest percentages of highest (0.2%), moderately high (30.4%), and moderate (26.1%) at-risk areas for pandemic spread (Table S7). India follows, with 7.5% of its land area classified at moderate or moderately high risk for pandemic spread. Pakistan and China are next with 3.0% of their respective country areas recorded to be at high risk of pandemic spread. These results highlight that countries with higher population densities and are closest to high eRIDE and PAR areas are at most risk of a possible pandemic.

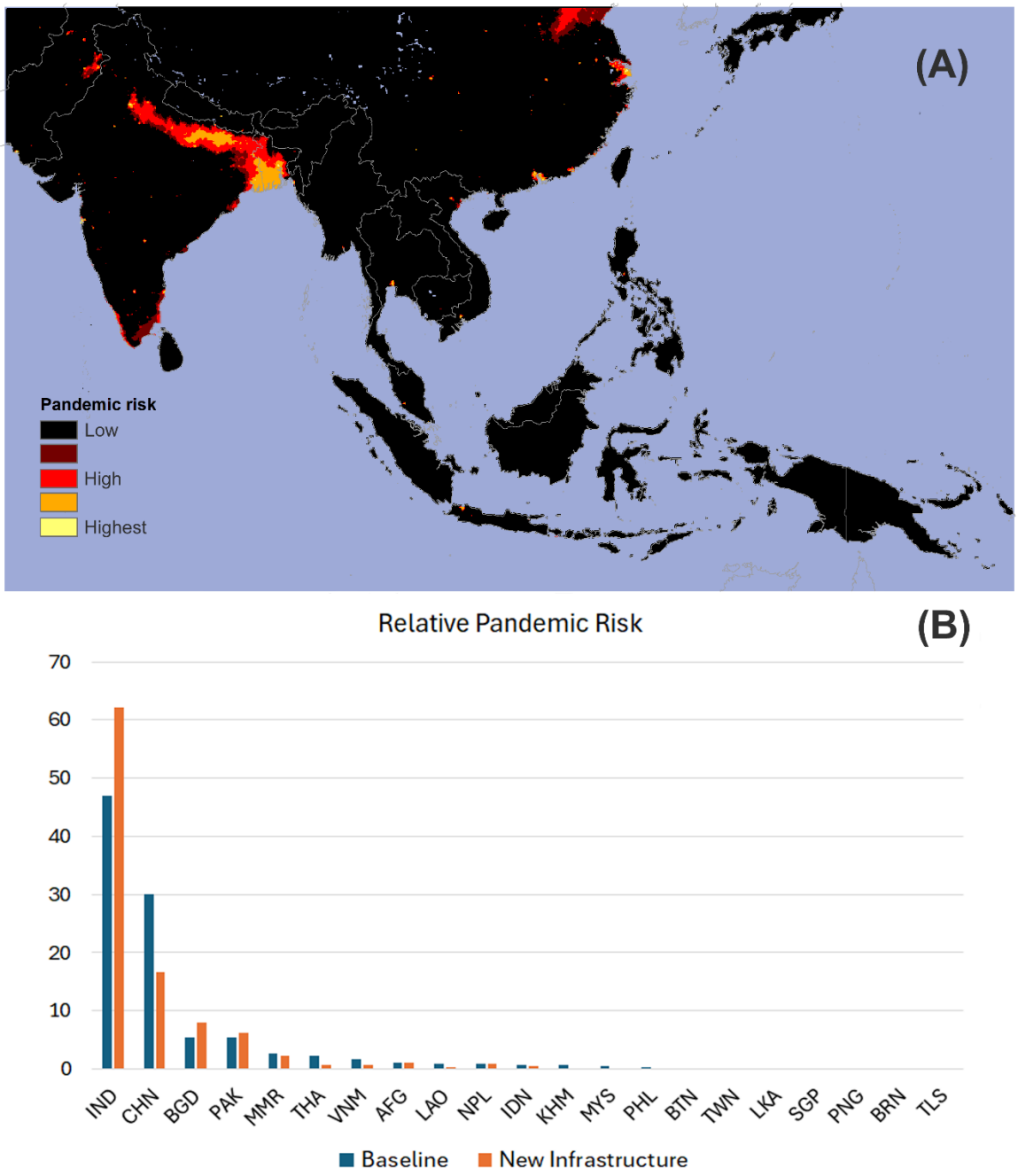

Figure 4. Simulated Pandemic Risk from Zoonotic Agents in Rhinolophid Bats of Tropical East Asia. Depicted here are the (**A**) map of pandemic risk areas under baseline scenario (discrete color bands in the legend follow an exponential scale), and (**B**) index rankings per country under baseline (blue) and new infrastructure (orange) scenarios, derived from the sum of pandemic risk scores within each country's border.

Increased fragmentation from existing and planned infrastructure scenario

Introducing road networks over the habitat increased fragmentation generally across all countries when compared to baseline scenario values (Table S2). All countries/territories experienced a decrease in mean patch area and patch cohesion index values compared to baseline values, and all except Bangladesh had a decline in their largest patch index values. China ranked first in terms of highest habitat fragmentation across first (baseline) and second (baseline + new infrastructure) scenarios. The most dramatic change is from Papua New Guinea, which experienced a +335.1% increase in number of patches concurrently with a -83.1% decrease in mean patch area and a -48.9% decline in its largest patch index value.

The relative eRIDE index rankings in the second scenario remain mostly unchanged when compared to the baseline scenario, with only minor redistributions in values between countries (Figure 2a). However, hotspots in specific regions were revealed by risk categorization and grid-wise spatial comparisons between the first and second scenarios (Figure 5; Table 1). In mainland Asia, the largest increases in combined high-risk areas were observed in Bhutan (+21.2%), followed by northeast India (+3.1%), western Myanmar (+1.8%) and Vietnam (+0.8%). In insular Asia, Taiwan observed a +11.4% increase in moderate risk areas, while Indonesia had a +5.8% increase in combined high-risk areas distributed among its islands of Kalimantan (Borneo), Sumatra, and Sulawesi. In Papua New Guinea, a +6.6% increase was observed. These hotspots occur in forest areas where existing and planned road networks are located (Figure 6).

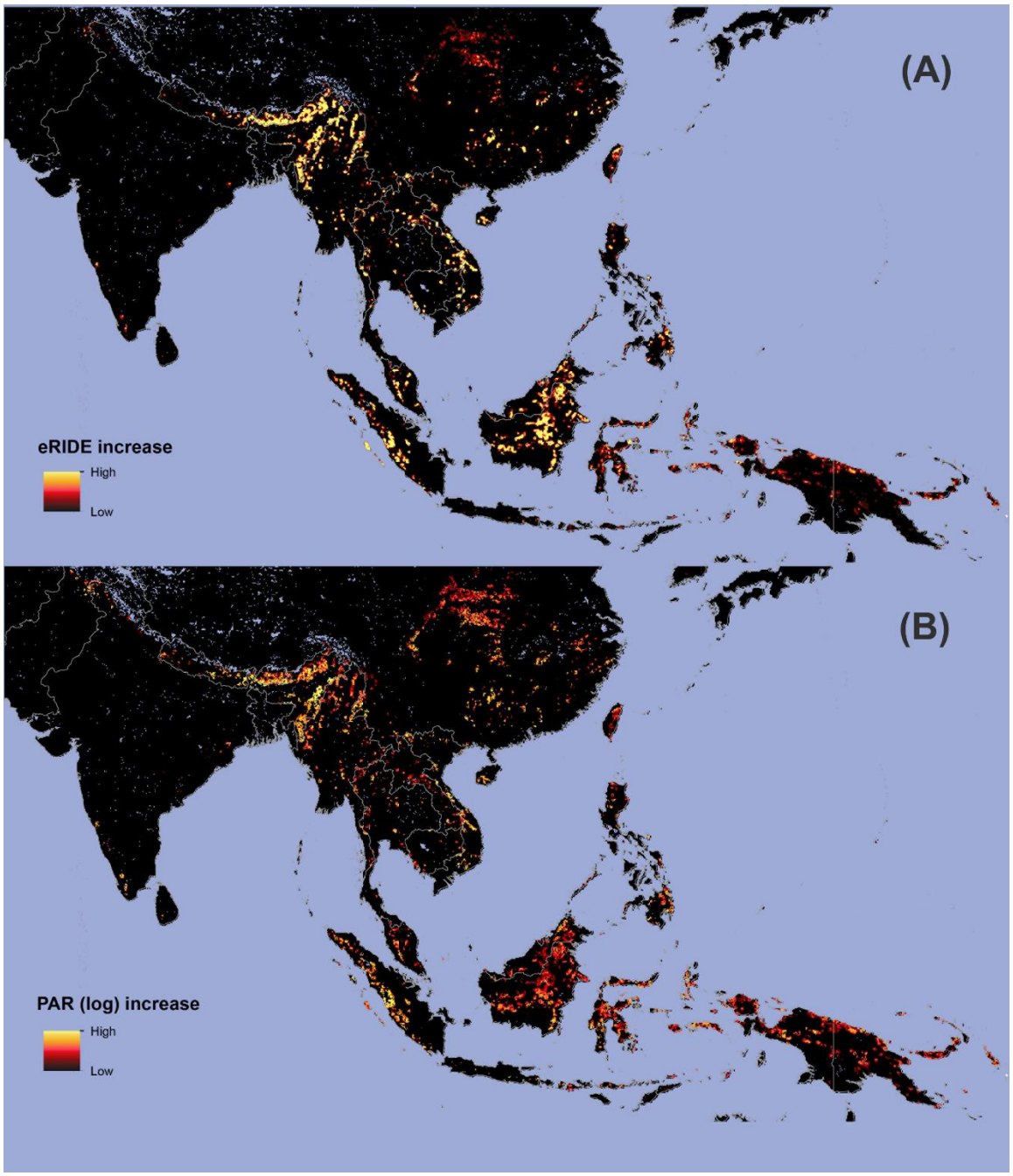

Figure 5. Changes in eRIDE and PAR Scores in Tropical East Asia Under New Infrastructure Scenario. Maps depicting increases in (**A**) eRIDE and (**B**) PAR (log) scores under the new infrastructure (NI) scenario. Change maps were computed by subtracting the values of the NI scenario from the baseline. Colors transition from black to yellow to indicate stronger increases.

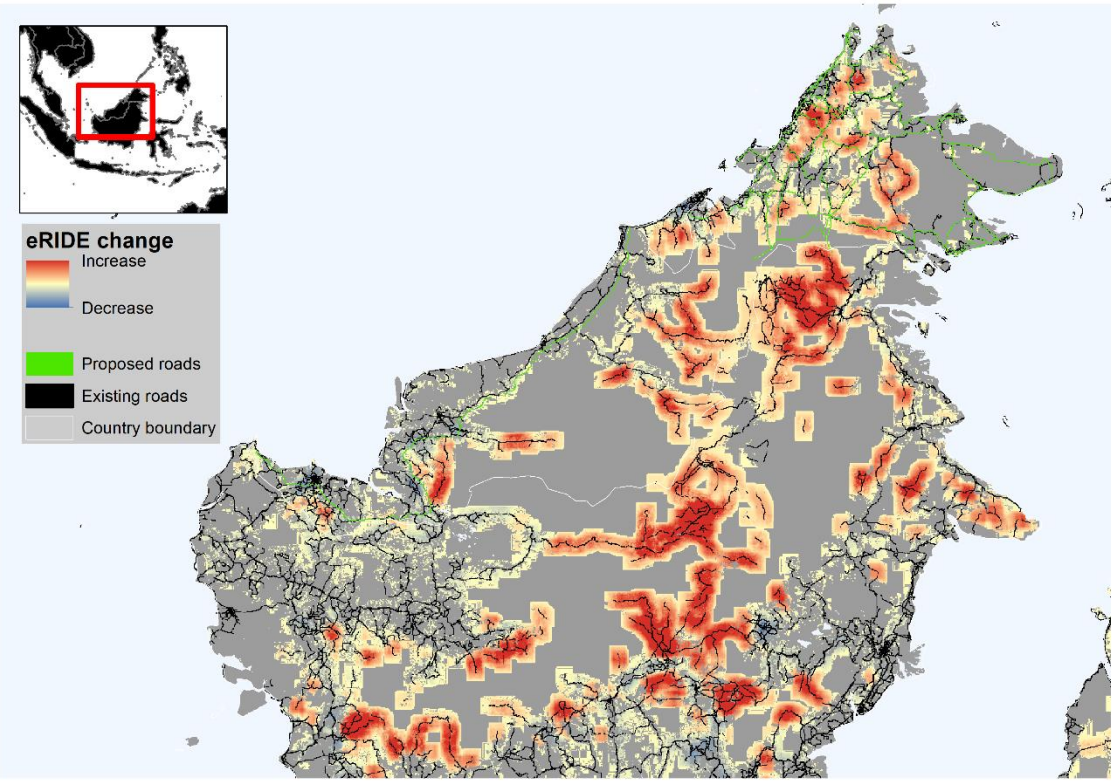

Figure 6. Changes in eRIDE in Borneo Island. Enlarged map of Borneo Island depicting changes in eRIDE values under the new infrastructure scenario. Increased eRIDE values are depicted here in yellows and reds, particularly along road networks (black and neon green lines), illustrating the potential impacts of infrastructure on tropical regions with intact forest habitats.

For PAR, China, India, and Indonesia still had the highest relative PAR scores under the second scenario (Table S4). The relative PAR scores for Vietnam (+0.6%), Myanmar (+1.6%), Thailand (+0.7%), Nepal (+0.2%), Laos (+0.4%), Bhutan (+0.3%), Bangladesh (+0.1%), and Papua New Guinea (+0.1%) also increased under the second scenario, although these changes barely affected the rankings (Figure 2b; Table S4). Risk categorization and spatial comparison between the scenarios revealed strong increases in high PAR areas for Sri Lanka (+11.1%), Taiwan (+8.1%) and Bhutan (+5.1%). The hotspots observed in the spatial comparisons were supported by the risk categorization (Table 1), particularly along northeast India (+2.6%), western Myanmar (+1.1%), central China (+3.6%), and Indonesia (+2.2%) (Figure 5b). Central Vietnam (+0.3%), peninsular Malaysia (+2.7%), Papua New Guinea (+2.3%), and southern Philippines (+4.5%) also registered moderate upward shifts.

The changes in PAR distributions intensified the relative pandemic risk values for the South Asian countries of India, Bangladesh, and Pakistan, as these countries registered increases in their pandemic risk scores (Figure 4; Table S4). India had a dramatic increase of +15%. China remained the second-highest country at risk due to its huge land area. Spatially, the risk patterns in the map are similar to the baseline simulation, with the majority of the highest risk areas still concentrated in the north-northeast India-Bangladesh corridor, as well as in the greater Guangzhou and Shanghai areas of China (Supplementary Figure S2). Relative to their respective land areas, Bangladesh registered the highest increase in pandemic risk areas (+9.8%), followed by (+1.8%), Pakistan (+1.3%), and Nepal (+0.2%) (Table 3).

Discussion

A OneHealth approach to spillover surveillance

There is a growing realization of the importance of integrating OneHealth perspectives into landscape management (*35*, *36*). New approaches which combine landscape parameters with the distribution of competent hosts can predict patterns of spillover risk. Here we demonstrate the use of a OneHealth approach to predict potential spillover and pandemic risk hotspots in tropical East Asia. Using the estimated risk of infectious disease emergence (eRIDE) and population-at-risk (PAR) indices, which are models that utilize the relationships between species richness, habitat fragmentation metrics and human population density in determining spillover hotspots, we found that Indochina and southern China are of highest risk for spillover in Asia due to their high Rhinolophid species richness alongside dense human populations. A subsequent pandemic spread network model we applied also revealed that South Asia, specifically Bangladesh and northeast India, has the highest risk for a pandemic once spillover occurs in the hotspots, or if infected wildlife is potentially transported to urban centers.

Using an approach that incorporates the biological, environmental, and human aspects of health is useful in establishing baseline knowledge on spillover potential hotspots, including distribution of competent hosts and natural interfaces for spillover without initially needing immunological or viral data. Spillovers into human populations require a virus to spill into humans (often via an intermediate host) and then spread from human-to-human, which is not only rare, but also is more likely to happen in areas where human populations have not acquired immunity (*37*). Rates of SARS-related coronaviruses from Southeast Asian bats have been previously examined, but such

studies may not accurately capture species ranges or the landscape dynamics that should be considered (*33*). Localized spillovers potentially remain underreported due to factors such as the lack of human-to-human transmission, the presence of acquired immunity preventing case mortalities, or inadequate reporting and identification in rural areas (*20*). This suggests that whilst existing studies on viral surveillance provide valuable insights, they may overlook potential spillover hotspots, as the bias in the data in these studies may not adequately represent where spillover events are likely to occur in the landscape. Thus, integrating species ecology and limitations into analysis is essential, as the ecology of vectors has profound implications for transmission pathways, or understanding how to manage and mitigate risk.

Direct use of competent hosts in modeling risk

Understanding potential spillover locations in the landscape requires identifying interfaces between humans and competent hosts. Competent hosts such as rodents and birds act as reservoirs for pathogenic viruses and bacteria (*14*, *38*, *39*). By focusing on the distribution of these competent hosts, we can pinpoint natural interfaces for spillover events. Rhinolophid bats, which are known reservoirs of coronaviruses related to SARS and COVID-19 (*6*, *22*), were directly studied to look at their potential for zoonoses. Utilizing the eRIDE and PAR models, which are most effective in systems with defined edges such as forests (*9*), we identified spillover hotspots where bat movement between forest fragments could lead to pathogen transmission to humans and other hosts.

The eRIDE (potential pathogen emergence) hotspots identified coincided with forested regions of high Rhinolophid species richness (Supplementary Figure S1) but also in areas with high fragmentation, aligning with previous studies mapping potential coronavirus host bat species in Southeast Asia (*33*, *40*), particularly in Southern China, eastern Myanmar, and northern Laos. Recent investigations have uncovered the presence of SARS-CoV-like coronaviruses in bats in these regions despite limited sampling (*6*, *24*, *33*). The diverse Rhinolophid bat communities in these regions can facilitate interactions between species, potentially leading to the mixing of potential zoonotic viruses. Given that individual bats can host multiple viruses concurrently and tend to roost in densely populated fragmented habitats (*6*, *41*), the risk of pathogen spillover to humans in these habitat edges are higher. However, further work is needed to better describe Rhinolophid species and their interactions across the region (*42*) to facilitate a clearer understanding of viral dynamics, especially in how they vary across space and time.

Impact of population density in pandemic risk

The high similarity between the high eRIDE and PAR hotspots demonstrates that populations in Asia are at proximity to high spillover risk exposure areas. This is in contrast with the original application of these models in Africa, which found that potential risk transmission areas (i.e. high eRIDE risk) are sparsely populated and distant from the high PAR areas, and thus highlighted the role of population centers in disease emergence and transmission (*9*). Our use of the models in Asia provides a more localized context wherein the proximity of nearby population centers could mean that zoonotic diseases from Rhinolophids could possibly be transmitted from animal to people more rapidly. In Asia, there is steadily increasing population density in peri-urban areas where there are potential interactions between wildlife and domesticated animals and humans, therefore higher proximity between zoonotic systems (*43*–*45*). Migration of human populations or changing patterns of tourism can increase exposure of naïve human populations to pathogens, thus increasing chances for outbreak when spillover happens (*46*, *47*). Furthermore, migrating human populations may drive wildlife trade, wildlife farming, and their associated risks of spillover (*48*, *49*). Wildlife farming for fur and culinary consumption provide a major risk for potential zoonotic spillovers (*50*, *51*). These activities may be linked to the trade and illegal trafficking of wildlife, as evidenced by instances where raccoon dogs in Chinese markets are frequently native (possibly wild-caught) rather than farmed species (*52*). It is therefore crucial to understand the placement of these farms to implement rigorous biosecurity monitoring measures.

In terms of pandemic spread post-spillover event, our network model results showed that the high-risk areas were aggregated around dense population centers, notably in eastern India and Bangladesh as well as the megacities in eastern (Shanghai) and southern (Guangdong) China. These further demonstrate the effect of population density and land transport networks in moving potentially zoonotic viruses from their sources as evidenced in the PAR hotspots, and akin to what has been observed in previous cases of zoonoses, such as for Marburg and Ebola in the African continent. For instance, the index case for the 2013 Ebola epidemic in West Africa was traced to a Guinean village already heavily modified by human activity, in contrast to earlier cases where initial spillover likely occurred in villages closer to core forest areas (*8*, *53*). Similarly, the index case for a Marburg virus outbreak in 2012 in Uganda was attributed to a traveler who got infected upon returning from his hometown (*54*). eRIDE predictions are consistent with risk emergence hotspots with high spatial resolution for *Ebolavirus* in Africa, a region where spillover data for Ebola virus disease is more widely tracked (*9*). This approach provides a non-invasive and cost-

efficient strategy to localize potential risk areas without resorting to lethal methods for pathogen detection in bats, a practice documented in previous studies (e.g. *55*, *56*), and can be cross validated by field surveys, such as the use of tarpaulins to collect urine for testing in saves. The outcomes derived from our models can provide guidance for governmental organizations in the designated high-risk regions to formulate contingency measures in anticipation of potential recurrence of a coronavirus spillover event.

Fragmentation increases spillover risk in Asia

Increasing habitat fragmentation resulting from the development of road networks may increase spillover risks, as increased eRIDE and PAR scores were observed in forested areas of western Myanmar, Bhutan, Borneo, and New Guinea. High PAR scores in the northern portions of South Asia have particularly led to the high pandemic spread risk score of Bangladesh and India, given especially the high population density and connectivity of this area to both South and mainland Southeast Asia, where eRIDE hotspots are concentrated. Additionally, planned infrastructure in Bornean landscapes will fragment important landscapes and drive biodiversity declines (*34*, *57*). The same patterns of decline are likely to be observed in New Guinea, as development along the Trans-Papuan highway has already led to significant loss in forest areas, and subsequently, this region's remarkable biodiversity (*58*).

Habitat degradation resulting from activities such as deforestation, agricultural expansion, and urbanization leads to greater pathogen spillover by creating edge effects that increase interspecies contact and the transmission of zoonotic pathogens (*9*, *59*). These edge effects serve as transition zones where wildlife, domestic animals, and humans come into closer contact, heightening the risk of spillover events (*44*). The loss of biodiversity from habitat fragmentation increases the risk of spillovers, as decreasing habitat quality reduces species diversity and abundance, reversing the "dilution effect" that normally helps lower pathogen prevalence due to a higher number of susceptible host species (*10*, *60*). This was demonstrated in a study on CoV prevalence in bat communities in Ghana, where higher CoV prevalence and infection likelihood were observed in communities with lower bat diversity resulting from disturbances in habitat structure, thus leading to increased exposure to diseases by humans or greater interface with potential generalist intermediate hosts (*35*). This highlights the buffering effect of biodiversity, and proactive strategies to enhance habitat connectivity and extent must be implemented to maintain healthy wildlife populations and reduce the interfaces where spillover is most probable.

Pathogen spillover increases during land conversion, particularly at intermediate levels of habitat loss where there is a large population of competent hosts still present in core habitats alongside susceptible hosts in human-modified landscapes (*13*, *59*). Intermediately fragmented areas contain higher numbers of competent hosts in the core habitats, leaving naïve populations exposed in the surrounding matrix (*61–63*). This scenario is evident in cases such as in Henipavirus outbreaks in Bangladesh and rabies incidences in cattle associated with deforestation and habitat fragmentation (*37*, *64*). This may be linked to high stress to wildlife populations as well as large interfaces between wildlife and humans, livestock or domestic animals. Therefore, addressing habitat fragmentation is crucial in regions like southwest China, known for high rates of coronavirus transmission risk and being a major habitat for bats identified as betacoronavirus reservoirs (*65*), but where fragmentation of natural habitats is also high (*66*, *67*).

Maintaining the core of habitats is essential for reducing habitat perimeters and minimizing contact zones where disease transmissions can occur (*9*). The growth of infrastructure and increasing edge density in these habitats will make these areas higher-risk zones for pandemic spread in neighboring regions. Preventing further fragmentation is crucial, as there are already observed shifts in global bat diversity due to climate change (*68*), which could exacerbate viral transmission risk between species (*7*). Furthermore, spillover risk is not static over time. Factors such as increasing extreme climate events, interacting with habitat loss and agricultural expansion, play a direct role in driving spillover events, like those seen in the case of Hendra (*69*) and Nipah viruses (*70*, *71*). Recognizing and understanding these interconnected threats can facilitate actions to break the transmission chains (*72*). Maintaining intact habitats, especially in the face of multiple other stressors is clearly critical not only for maintaining biodiversity, but also to reduce the risk of spillover, and thus should be seen as a component of maintaining ecological security.

Summary and next steps

Our work demonstrates an application of the OneHealth paradigm in addressing the threat of zoonotic spillover events from Rhinolophid bats in Asia, a region identified as the epicenter of recent epidemics, including the devastating global COVID-19 pandemic which has already claimed over 7 million lives worldwide. By identifying hotspots and advocating for urgent implementation of mitigation measures, we emphasize the importance of a multidisciplinary and collaborative approach in safeguarding public health and ecosystem integrity. Our results suggest that there are

high spillover risk hotspots concentrated in Indochina and Southern China, which could then propagate across the region, particularly affecting the densely populated areas of northern India and Bangladesh.

Whilst model validation is challenging due to the underreporting of coronavirus spillover events in Asia (*20*) and the probable high levels of immunity in rural human populations, understanding the potential for spillover provides the means for targeting actions to stem the potential for spillover risk. Our findings can offer guidance for targeted resource allocation in epidemiological surveillance of identified high-risk areas, presenting a collaborative approach to result validation and mitigation of impacts on bat populations and viral disease transmission risks. Furthermore, frameworks like these can reflect the diverse species ecophysiology across different taxa, exemplified here by the Rhinolophids (known for their photophobic behavior and preference for high-density habitats), and can also evaluate seasonal fluctuations (*19*). This proactive and cost-effective strategy can address potential sources of the issue preemptively, rather than reactively responding to spillover events.

The methods presented in our study can be further enhanced by including seasonality factors, especially when linked to seasonal biological phenomena such as pregnancy and hibernation, as well as land use and anthropogenic climate change dynamics in the models. The pandemic spread network model can be further refined by including transport links between hubs for a more accurate simulation of disease spread. Additionally, the inclusion of wildlife farm locations, particularly those housing known competent hosts like small carnivores, can enhance the model's effectiveness. These improvements can prove essential in potential applications when determining zoonoses for different taxonomic groups and regions, given calls for further explorations of viruses with zoonotic potential outside the public health priorities of Sub-Saharan Africa and Southeast Asia, where pandemics have more recently emerged (*73*).

Our work lays a foundation for future research that explores the integration of additional factors for enhanced predictive capabilities and tailored surveillance efforts in vulnerable regions. Furthermore, we highlight the vulnerability of human population centers across the region and the heightened risk accompanying infrastructural growth. Notably, SARS-CoV2 is only one of several betacoronaviruses which has emerged from Southeast Asia, with Rhinolophid bats as a probable source. Preventing future epidemics necessitates interventions to mitigate this risk, integrate

OneHealth approaches into planning, and reduce interactions between stressed wildlife and potential intermediate species of bat-borne pathogens.

Materials and Methods

To locate areas with high potential for novel disease emergence arising from horseshoe bat richness and habitat fragmentation, we first generated maps that display both using the following methods. These approaches were based on Wilkinson et al. (2018) but adapted for the context of the South and Southeast Asian region, and for a more specific approach to coronaviruses.

Assessment of habitat fragmentation in Asia through analysis of remote sensing products

Land-cover maps that exist typically overestimate the amount of forest in the region due to their overreliance on canopy cover as the sole metric to identify forest vs non-forest (*74*, *75*). This is especially obvious in Southeast Asia, where there is a significant coverage of rubber and palm oil plantations yet are not identified as separate land-cover classes in existing products (e.g. GLAD Land Cover) due to the challenge of distinguishing types of tree-cover using basic mapping approaches. In addition, in drier climates in the region, natural forests may be both shorter and sparse (*76*), thus to accurately map forests and distinguish them from plantations, different thresholds must be set based on precipitation. We therefore mapped remaining forest areas in tropical East Asia using a combination of remotely sensed canopy height and modeled precipitation data following an approach used in B. V. Li et al. (2016) to accurately map forests across the same region. First, we obtained canopy height data from ETH Global Sentinel-2 10m Canopy Height data for 2020 covering the entire region (66° to 156° E longitude, -16° S to 36° N latitude). Data was downloaded through Google Earth Engine, after resampling from 10 m to 1 km (download date: 8 Aug 2023). We chose 1 km as the resolution as it corresponds closest to the highest available resolution for climate data (30”, which is approx. 1 km at the equator). Annual precipitation data was obtained from CHELSA ver. 2.1 (download date: 6 Sep 2022).

Given the dependence of Rhinolophid bats on intact forest regions, we needed to delineate forest from non-forest in the region so that fragmentation could be assessed. Owing to the precipitation differences between dry-deciduous and wetter forests, we separated the region between these two climate regions based on biomes delineated in the Ecoregions 2017 map (*78*), and precipitation thresholds used in (*77*). We then applied the following criteria to classify forest pixels from the canopy height map:

1. Tropical areas with precipitation values ≥ 1800 mm/year and with canopy height ≥ 20 m were classified as forest;

2. Tropical areas with precipitation values < 1800 mm/year and with canopy height ≥ 25 m were classified as forest;

3. Temperate areas with precipitation values ≥ 600 mm/year and with canopy height ≥ 20 m were classified as forest

In order to mask out plantation areas that fall under the canopy height limits we set for each region, we used plantation map data obtained from multiple sources. First, we downloaded the Spatial Database of Planted Trees (SDPT) version 1.0 compiled by Global Forest Watch (GFW), which categorizes plantations of native or introduced species worldwide based on supervised classification or manual delineation of satellite imagery (*79*, downloaded on 15 Aug 2023). We then supplemented this by generating a land-cover mask of all cropland and plantation areas obtained from the Thai government (*80*) and a study which classified rubber plantations in Yunnan Province in China for 2016 (*66*). All geoprocessing was performed in R version 4.0.5 using the *raster* package.

Lastly, we conducted an area-adjusted pixel-based accuracy assessment on the forest map generated by creating a confusion matrix. From this matrix, we calculated the overall, user's, and producer's accuracy metrics for the forest and non-forest classes. To derive this, we randomly sampled points from the forest and non-forest classes on the map product. Each point was then visually assessed for its classification accuracy by comparing it with high-resolution imagery from ESRI using ArcMap 10.4. The results were then compiled into a confusion matrix to quantify the classification performance. To assess the uncertainty associated with each estimation, we computed error-adjusted area estimations and confidence intervals for each class (*81*). The resulting forest map demonstrated an overall accuracy of 96.1%, with producer's accuracy for the classes ranging from 86.3 to 100%, and user's accuracy ranging from 78.0 to 98.0% (Table S1).

Mapping Rhinolophid species richness in Asia

We used Rhinolophid species richness as a metric for potential interactions between competent hosts in the forest fragments. We computed species richness by overlapping the suitable habitats for Rhinolophid bats, which were predicted using Maxent (*82*), a widely used algorithm in

modeling species distributions due to its generally good capability of predicting suitable habitats given a minimum number of species records (*83*).

Species points sources and processing

Species occurrence points for bats from the Rhinolophidae family within the study region were obtained from the dataset used in (*84*), which is a combination of data from the Global Biodiversity Information Facility (*85, 86*), the DarkCideS database (*87*), and field sampling. We also compiled additional points for Indonesia from multiple published datasets (see Supplementary S3). Taxonomic names were then updated using the Bats of the World database (batnames.org, accessed on 1 Oct 2023). A total of 7,885 data points across 59 Rhinolophidae bat species were compiled.

To avoid spatial autocorrelation, a spatial thinning algorithm that retains one occurrence point per species for each grid cell at 30" resolution (0.008333°) was applied. Potentially invalid coordinates were also identified and removed using the clean_coordinates() function of the CoordinateCleaner package in R. Invalid points include those that might be outliers, within country capitals or country centroids, within research institutions and botanical gardens, or outside land masses. After cleaning, we retained species with more than 15 points for modeling, leaving the final number of species at 44.

Environmental predictors

To predict the bats' suitable habitat, a suite of environmental predictors important to bat ecology was selected. For climate, we obtained bioclimatic variables from CHELSA version 2.1 (*88*), and a Global Aridity Index from the Global Aridity Index and Potential Evapo-Transpiration (ET0) Database v3 (*89*). Due to the lack of high-resolution global karst maps essential to locate caves which bats inhabit, we represented karst habitats by using a Depth to bedrock (R horizon) layer obtained from SoilGrids 2.0 (*90*), with the assumption that karst areas are in regions with shallow bedrock depths owing to the thin soils in these formations.

To represent vegetation cover, we used two layers. First, we obtained the ETH Global Canopy Height 2020 product, which estimated vegetation heights globally from remote sensing data (*91*). This is useful to differentiate between natural and cultivated vegetation types in which the bats inhabit. Second, we used a Normalized Difference Vegetation Index (NDVI) layer obtained from the MOD13A2 V6.1 Terra product set released by MODIS (*92*) to represent vegetation productivity. Since this image satellite product is released every 16 days, we computed the mean

NDVI for the year 2020 using all available imagery for that year. Both these vegetation layers were hosted, processed, and downloaded through Google Earth Engine Data Catalog (downloaded on 20 Sep 2023).

We produced a "distance from water bodies" layer, in which each grid cell's distance to the nearest freshwater body was calculated using a freshwater bodies layer obtained from the MERIT Hydro Global Hydrography dataset (*93,* downloaded on 30 Aug 2023). We first processed the available freshwater bodies layer into binary (i.e. water body vs land), then computed the Euclidean distance of each land grid cell to the nearest water body cell. Processing for this was performed in ArcMap version 10.4.

All environmental predictors were then resampled to 30" resolution, stacked together, and checked for multicollinearity using Spearman's rank correlation test. Predictors with Spearman's $r > 0.7$ were removed from the model, and the following predictors were retained: mean annual temperature (Bio1), temperature annual range (Bio7), precipitation of wettest month (Bio13), precipitation seasonality (Bio15), aridity index, depth to bedrock, distance to water bodies, and vegetation height.

Maxent modeling

Maxent was used to model suitable habitats of the Rhinolophid bat species. Prior to each species run, 10,000 background points were randomly generated from within a 500-km buffer region of the species' occurrence points. The ENMEVal package was then used to test different combinations of feature classes (linear, quadratic, and hinge) and regularization multipliers (1 to 5), and the model with the lowest delta AIC score was selected as the most optimal and predicted to space to visualize suitable habitats (*94*). Model accuracy tests utilized the Area Under the Curve (AUC) and the True Skill Statistic (TSS; *95*). All species models yielded good scores, with mean AUC score at 0.861, ranging from 0.780 to 0.951, while TSS scores were generally fair to good, with a mean of 0.534 and ranging from 0.278 to 0.875 (Table S3).

Each continuous species suitability map was then converted into a binary presence-and-absence map using the 10-percentile training threshold score for each species. To avoid overpredicting the suitable habitats of the bats, the binary maps were clipped according to the biogeographic regions each species has been recorded in, the native ranges based on the distribution of point records, and species range maps published by IUCN (*96*). Lastly, the clipped rasters were summed to obtain

species richness scores. All processing was performed using R ver. 4.0.5 unless otherwise specified.

Mapping potential spillover risk hotspots

To determine potential disease risk hotspots from the Rhinolophid bat populations in remaining habitat fragments, we used an approach from Wilkinson et al. (2018) called the estimated risk of infectious disease emergence, or eRIDE, index (*9*). In this model, the potential disease risk is estimated based on the diversity of disease-causing species within a habitat patch. It directly correlates species diversity within habitat patches with exposure to human populations, quantified using the edges of the habitat fragments. The model assumes that the number of potential zoonotic agents within the habitat has a direct, linear relationship with fragment diversity, such that the total hazard from novel pathogens is proportional to patch biodiversity. In this case, we represented diversity using the viral populations hosted by the Rhinolophids in each patch. The model also assumes that the area where human populations comes into contact with the habitat is represented by the perimeter of the patches. Thus, the more habitat fragment edges there are, the higher the risk becomes.

To compute eRIDE, we first identified the edge pixels of each fragment, then the focal sum of edge pixels within a 20 x 20 moving window was computed for each grid cell following Wilkinson et al. (2018). The eRIDE index of each cell was then computed as the product of its focal sum of edge pixels and bat species richness score. To identify which populations are at most risk from potential emerging infectious diseases, an estimated population at risk (PAR) index was computed as the product of each cell's eRIDE index and population density. The relative eRIDE and PAR percent scores for each country/territory were then computed as the sum of eRIDE or PAR for each country/territory divided by the total eRIDE or PAR value across the entire modeling region. To assess the categorical risk for each location, the eRIDE and PAR (log) values was reclassified into five categories (low, moderately low, high, moderately high, highest risk) to represent the different levels of risk using the respective geometric progression intervals of the eRIDE and PAR (log) values across the whole region. Unconstrained individual population density data for 2020 for all Asian countries within our mapping domain was obtained from WorldPop (https://hub.worldpop.org/project/categories?id=18, downloaded on 11 July 2023).

Pandemic risk mapping

Potential pandemic hotspots were then identified using a network model of pandemic spread based on human density and connectivity (*9*). First the raster was aggregated from 1-km to 10-km resolution, then the pixel grid was converted into a network using 4-connectivity, with each grid cell representing nodes. Pandemic spread was assumed to likely travel faster between more densely populated places, thus the edge weights between adjacent pixels were computed as the inverse of the product of the population densities of each pixel.

The likelihood for pandemic spread between corresponding pixels *x* and *y* was then assessed by first determining the shortest distance *s(x, y)* on the graph between the two nodes, which was computed using Djikstra's algorithm. The relative chance of pandemic spread *ps* for any pixel *y* was then computed as

$$ps(y) = \sum_{x} \mathrm{PAR}(x) s(x, y)$$

where the sum from all potential source pixels *x* is obtained. The relative pandemic risk percent score for each country/territory was then computed as the sum of the pandemic risk score for each country/territory divided by the total pandemic risk score across the entire modeling extent. To assess the categorical risk for each country, the pandemic spread risk scores were reclassified into five categories (low, moderately low, high, moderately high, highest risk) to represent different levels of risk using the geometric progression intervals of the pandemic risk scores across the whole region. The R packages *raster*, *tidygraph*, and *igraph* were used for these analyses.

Increased fragmentation from existing and planned infrastructure scenario

Existing and planned infrastructure are known to introduce further fragmentation to natural habitats (*97*). To investigate the possible effect of adding infrastructure to spillover risk, the models were also run under a second scenario wherein existing and planned infrastructure are applied to mask the existing forest cover map. Existing infrastructure data (e.g. road and rail networks) for the entire region were obtained from OpenStreetMaps (downloaded on 29 March 2024). Planned infrastructure data were also downloaded from various sources for China, Indonesia, Malaysia, India, and Papua New Guinea (see Supplementary for complete list of sources). After processing these into rasters, the infrastructure layers were masked from the existing forest cover map using

raster calculator. The models for eRIDE, PAR and pandemic spread were then run using the fragmented forest cover map.

Fragmentation statistics for each country were also computed from the two scenarios (baseline + new infrastructure). The number of fragments, fragment size (as mean patch area and largest patch index), geometric complexity (as mean patch shape ratio), physical connectedness (patch cohesion index), and edge density were all quantified using the *landscapemetrics* package in R.

References

1. K. E. Jones, N. G. Patel, M. A. Levy, A. Storeygard, D. Balk, J. L. Gittleman, P. Daszak, Global trends in emerging infectious diseases. *Nature* **451**, 990–993 (2008).

2. L. H. Taylor, S. M. Latham, M. E. J. Woolhouse, Risk factors for human disease emergence. *Philosophical Transactions of the Royal Society of London. Series B: Biological Sciences* **356**, 983–989 (2001).

3. B. A. Han, A. M. Kramer, J. M. Drake, Global Patterns of Zoonotic Disease in Mammals. *Trends in Parasitology* **32**, 565–577 (2016).

4. K. J. Olival, P. R. Hosseini, C. Zambrana-Torrelio, N. Ross, T. L. Bogich, P. Daszak, Host and viral traits predict zoonotic spillover from mammals. *Nature* **546**, 646–650 (2017).

5. Z. Wu, Y. Han, B. Liu, H. Li, G. Zhu, A. Latinne, J. Dong, L. Sun, H. Su, L. Liu, J. Du, S. Zhou, M. Chen, A. Kritiyakan, S. Jittapalapong, K. Chaisiri, P. Buchy, V. Duong, J. Yang, J. Jiang, X. Xu, H. Zhou, F. Yang, D. M. Irwin, S. Morand, P. Daszak, J. Wang, Q. Jin, Decoding the RNA viromes in rodent lungs provides new insight into the origin and evolutionary patterns of rodent-borne pathogens in Mainland Southeast Asia. *Microbiome* **9**, 18 (2021).

6. H. Zhou, J. Ji, X. Chen, Y. Bi, J. Li, Q. Wang, T. Hu, H. Song, R. Zhao, Y. Chen, M. Cui, Y. Zhang, A. C. Hughes, E. C. Holmes, W. Shi, Identification of novel bat coronaviruses sheds light on the evolutionary origins of SARS-CoV-2 and related viruses. *Cell* **184**, 4380-4391.e14 (2021).

7. C. J. Carlson, G. F. Albery, C. Merow, C. H. Trisos, C. M. Zipfel, E. A. Eskew, K. J. Olival, N. Ross, S. Bansal, Climate change increases cross-species viral transmission risk. *Nature* **607**, 555–562 (2022).

8. M. C. Rulli, M. Santini, D. T. S. Hayman, P. D'Odorico, The nexus between forest fragmentation in Africa and Ebola virus disease outbreaks. *Sci Rep* **7**, 41613 (2017).

9. D. A. Wilkinson, J. C. Marshall, N. P. French, D. T. S. Hayman, Habitat fragmentation, biodiversity loss and the risk of novel infectious disease emergence. *Journal of The Royal Society Interface* **15**, 20180403 (2018).

10. F. Keesing, R. S. Ostfeld, Impacts of biodiversity and biodiversity loss on zoonotic diseases. *Proc. Natl. Acad. Sci. U.S.A.* **118**, e2023540118 (2021).

11. R. K. Plowright, P. Eby, P. J. Hudson, I. L. Smith, D. Westcott, W. L. Bryden, D. Middleton, P. A. Reid, R. A. McFarlane, G. Martin, G. M. Tabor, L. F. Skerratt, D. L. Anderson, G. Crameri, D. Quammen, D. Jordan, P. Freeman, L.-F. Wang, J. H. Epstein, G. A. Marsh, N. Y. Kung, H. McCallum, Ecological dynamics of emerging bat virus spillover. *Proceedings of the Royal Society B: Biological Sciences* **282**, 20142124 (2015).

12. C. K. Glidden, N. Nova, M. P. Kain, K. M. Lagerstrom, E. B. Skinner, L. Mandle, S. H. Sokolow, R. K. Plowright, R. Dirzo, G. A. D. Leo, E. A. Mordecai, Human-mediated impacts on biodiversity and the consequences for zoonotic disease spillover. *Current Biology* **31**, R1342–R1361 (2021).

13. R. Gibb, D. W. Redding, K. Q. Chin, C. A. Donnelly, T. M. Blackburn, T. Newbold, K. E. Jones, Zoonotic host diversity increases in human-dominated ecosystems. *Nature* **584**, 398–402 (2020).

14. Y. Kane, A. Tendu, R. Li, Y. Chen, E. Mastriani, J. Lan, A. Catherine Hughes, N. Berthet, G. Wong, Viral diversity in wild and urban rodents of Yunnan Province, China. *Emerging Microbes & Infections* **13**, 2290842 (2024).

15. F. Keesing, R. S. Ostfeld, Emerging patterns in rodent-borne zoonotic diseases. *Science* **385**, 1305–1310 (2024).

16. V. Gorbunova, A. Seluanov, B. K. Kennedy, The World Goes Bats: Living Longer and Tolerating Viruses. *Cell Metabolism* **32**, 31–43 (2020).

17. A. T. Irving, M. Ahn, G. Goh, D. E. Anderson, L.-F. Wang, Lessons from the host defences of bats, a unique viral reservoir. *Nature* **589**, 363–370 (2021).

18. T. J. O'Shea, P. M. Cryan, A. A. Cunningham, A. R. Fooks, D. T. S. Hayman, A. D. Luis, A. J. Peel, R. K. Plowright, J. L. N. Wood, Bat Flight and Zoonotic Viruses. *Emerg Infect Dis* **20**, 741–745 (2014).

19. P. Eby, A. J. Peel, A. Hoegh, W. Madden, J. R. Giles, P. J. Hudson, R. K. Plowright, Pathogen spillover driven by rapid changes in bat ecology. *Nature* **613**, 340–344 (2023).

20. L.-F. Wang, D. E. Anderson, Viruses in bats and potential spillover to animals and humans. *Curr Opin Virol* **34**, 79–89 (2019).

21. D. J. Becker, G. F. Albery, A. R. Sjodin, T. Poisot, L. M. Bergner, B. Chen, L. E. Cohen, T. A. Dallas, E. A. Eskew, A. C. Fagre, M. J. Farrell, S. Guth, B. A. Han, N. B. Simmons, M. Stock, E. C. Teeling, C. J. Carlson, Optimising predictive models to prioritise viral discovery in zoonotic reservoirs. *The Lancet Microbe* **3**, e625–e637 (2022).

22. W. Li, Z. Shi, M. Yu, W. Ren, C. Smith, J. H. Epstein, H. Wang, G. Crameri, Z. Hu, H. Zhang, J. Zhang, J. McEachern, H. Field, P. Daszak, B. T. Eaton, S. Zhang, L.-F. Wang, Bats Are Natural Reservoirs of SARS-Like Coronaviruses. *Science* **310**, 676–679 (2005).

23. M. Letko, S. N. Seifert, K. J. Olival, R. K. Plowright, V. J. Munster, Bat-borne virus diversity, spillover and emergence. *Nat Rev Microbiol* **18**, 461–471 (2020).

24. H. Zhou, X. Chen, T. Hu, J. Li, H. Song, Y. Liu, P. Wang, D. Liu, J. Yang, E. C. Holmes, A. C. Hughes, Y. Bi, W. Shi, A Novel Bat Coronavirus Closely Related to SARS-CoV-2 Contains Natural Insertions at the S1/S2 Cleavage Site of the Spike Protein. *Current Biology* **30**, 2196-2203.e3 (2020).

25. A. Chornelia, A. C. Hughes, The evolutionary history and ancestral biogeographic range estimation of old-world Rhinolophidae and Hipposideridae (Chiroptera). *BMC Ecol Evo* **22**, 112 (2022).

26. M. G. Walsh, Mapping the risk of Nipah virus spillover into human populations in South and Southeast Asia. *Trans R Soc Trop Med Hyg* **109**, 563–571 (2015).

27. A. Chaiyes, P. Duengkae, W. Suksavate, N. Pongpattananurak, S. Wacharapluesadee, K. J. Olival, K. Srikulnath, S. Pattanakiat, T. Hemachudha, Mapping Risk of Nipah Virus Transmission from Bats to Humans in Thailand. *EcoHealth* **19**, 175–189 (2022).

28. A. A. Cunningham, P. Daszak, J. L. N. Wood, One Health, emerging infectious diseases and wildlife: two decades of progress? *Philosophical Transactions of the Royal Society B: Biological Sciences* **372**, 20160167 (2017).

29. J. Zinsstag, E. Schelling, D. Waltner-Toews, M. Tanner, From "one medicine" to "one health" and systemic approaches to health and well-being. *Preventive Veterinary Medicine* **101**, 148–156 (2011).

30. M. C. Rulli, P. D'Odorico, N. Galli, D. T. S. Hayman, Land-use change and the livestock revolution increase the risk of zoonotic coronavirus transmission from rhinolophid bats. *Nat Food* **2**, 409–416 (2021).

31. T. Allen, K. A. Murray, C. Zambrana-Torrelio, S. S. Morse, C. Rondinini, M. Di Marco, N. Breit, K. J. Olival, P. Daszak, Global hotspots and correlates of emerging zoonotic diseases. *Nat Commun* **8**, 1124 (2017).

32. S. S. Morse, J. A. Mazet, M. Woolhouse, C. R. Parrish, D. Carroll, W. B. Karesh, C. Zambrana-Torrelio, W. I. Lipkin, P. Daszak, Prediction and prevention of the next pandemic zoonosis. *The Lancet* **380**, 1956–1965 (2012).

33. C. A. Sánchez, H. Li, K. L. Phelps, C. Zambrana-Torrelio, L.-F. Wang, P. Zhou, Z.-L. Shi, K. J. Olival, P. Daszak, A strategy to assess spillover risk of bat SARS-related coronaviruses in Southeast Asia. *Nat Commun* **13**, 4380 (2022).

34. S. Sloan, M. J. Campbell, M. Alamgir, A. M. Lechner, J. Engert, W. F. Laurance, Trans-national conservation and infrastructure development in the Heart of Borneo. *PLOS ONE* **14**, e0221947 (2019).

35. M. Meyer, D. W. Melville, H. J. Baldwin, K. Wilhelm, E. E. Nkrumah, E. K. Badu, S. K. Oppong, N. Schwensow, A. Stow, P. Vallo, V. M. Corman, M. Tschapka, C. Drosten, S. Sommer, Bat species assemblage predicts coronavirus prevalence. *Nat Commun* **15**, 2887 (2024).

36. R. L. Muylaert, D. A. Wilkinson, T. Kingston, P. D'Odorico, M. C. Rulli, N. Galli, R. S. John, P. Alviola, D. T. S. Hayman, Using drivers and transmission pathways to identify SARS-like coronavirus spillover risk hotspots. *Nat Commun* **14**, 6854 (2023).

37. J. H. Epstein, S. J. Anthony, A. Islam, A. M. Kilpatrick, S. Ali Khan, M. D. Balkey, N. Ross, I. Smith, C. Zambrana-Torrelio, Y. Tao, A. Islam, P. L. Quan, K. J. Olival, M. S. U. Khan, E. S. Gurley, M. J. Hossein, H. E. Field, M. D. Fielder, T. Briese, M. Rahman, C. C. Broder, G. Crameri, L.-F. Wang, S. P. Luby, W. I. Lipkin, P. Daszak, Nipah virus dynamics in bats and implications for spillover to humans. *Proceedings of the National Academy of Sciences* **117**, 29190–29201 (2020).

38. F. Bordes, A. Caron, K. Blasdell, M. de Garine-Wichatitsky, S. Morand, Forecasting potential emergence of zoonotic diseases in South-East Asia: network analysis identifies key rodent hosts. *Journal of Applied Ecology* **54**, 691–700 (2017).

39. E. S. Neves, I. H. Mendenhall, S. A. Borthwick, Y. C. F. Su, G. J. D. Smith, Detection and genetic characterization of diverse Bartonella genotypes in the small mammals of Singapore. *Zoonoses and Public Health* **65**, e207–e215 (2018).

40. R. L. Muylaert, T. Kingston, J. Luo, M. H. Vancine, N. Galli, C. J. Carlson, R. S. John, M. C. Rulli, D. T. S. Hayman, Present and future distribution of bat hosts of sarbecoviruses: implications for conservation and public health. *Proc. R. Soc. B.* **289**, 20220397 (2022).

41. A. Latinne, B. Hu, K. J. Olival, G. Zhu, L.-B. Zhang, H. Li, A. A. Chmura, H. E. Field, C. Zambrana-Torrelio, J. H. Epstein, B. Li, W. Zhang, L.-F. Wang, Z.-L. Shi, P. Daszak, Origin and cross-species transmission of bat coronaviruses in China. *Nat Commun* **15**, 10705 (2024).

42. A. Chornelia, J. Lu, A. C. Hughes, How to Accurately Delineate Morphologically Conserved Taxa and Diagnose Their Phenotypic Disparities: Species Delimitation in Cryptic Rhinolophidae (Chiroptera). *Front. Ecol. Evol.* **10** (2022).

43. E. Alirol, L. Getaz, B. Stoll, F. Chappuis, L. Loutan, Urbanisation and infectious diseases in a globalised world. *The Lancet Infectious Diseases* **11**, 131–141 (2011).

44. J. M. Hassell, M. Begon, M. J. Ward, E. M. Fèvre, Urbanization and Disease Emergence: Dynamics at the Wildlife–Livestock–Human Interface. *Trends in Ecology & Evolution* **32**, 55–67 (2017).

45. S. O. Vanwambeke, C. Linard, M. Gilbert, Emerging challenges of infectious diseases as a feature of land systems. *Current Opinion in Environmental Sustainability* **38**, 31–36 (2019).

46. A. Cascio, M. Bosilkovski, A. J. Rodriguez-Morales, G. Pappas, The socio-ecology of zoonotic infections. *Clinical Microbiology and Infection* **17**, 336–342 (2011).

47. T. Wu, C. Perrings, A. Kinzig, J. P. Collins, B. A. Minteer, P. Daszak, Economic growth, urbanization, globalization, and the risks of emerging infectious diseases in China: A review. *Ambio* **46**, 18–29 (2017).

48. J. E. Goldstein, I. Budiman, A. Canny, D. Dwipartidrisa, Pandemics and the human-wildlife interface in Asia: land use change as a driver of zoonotic viral outbreaks. *Environ. Res. Lett.* **17**, 063009 (2022).

49. A. Zhu, G. Zhu, Understanding China's wildlife markets: Trade and tradition in an age of pandemic. *World Development* **136**, 105108 (2020).

50. T. P. Peacock, W. S. Barclay, Mink farming poses risks for future viral pandemics. *Proceedings of the National Academy of Sciences* **120**, e2303408120 (2023).

51. J. Zhao, W. Wan, K. Yu, P. Lemey, J. H.-O. Pettersson, Y. Bi, M. Lu, X. Li, Z. Chen, M. Zheng, G. Yan, J. Dai, Y. Li, A. Haerheng, N. He, C. Tu, M. A. Suchard, E. C. Holmes, W.-T. He, S. Su, Farmed fur animals harbour viruses with zoonotic spillover potential. *Nature*, 1–6 (2024).

52. A. Crits-Christoph, J. I. Levy, J. E. Pekar, S. A. Goldstein, R. Singh, Z. Hensel, K. Gangavarapu, M. B. Rogers, N. Moshiri, R. F. Garry, E. C. Holmes, M. P. G. Koopmans, P. Lemey, T. P. Peacock, S. Popescu, A. Rambaut, D. L. Robertson, M. A. Suchard, J. O. Wertheim, A. L. Rasmussen, K. G. Andersen, M. Worobey, F. Débarre, Genetic tracing of market wildlife and viruses at the epicenter of the COVID-19 pandemic. *Cell* **187**, 5468-5482.e11 (2024).

53. A. Marí Saéz, S. Weiss, K. Nowak, V. Lapeyre, F. Zimmermann, A. Düx, H. S. Kühl, M. Kaba, S. Regnaut, K. Merkel, A. Sachse, U. Thiesen, L. Villányi, C. Boesch, P. W. Dabrowski, A. Radonić, A. Nitsche, S. A. J. Leendertz, S. Petterson, S. Becker, V. Krähling, E. Couacy-Hymann, C. Akoua-Koffi, N. Weber, L. Schaade, J. Fahr, M. Borchert, J. F. Gogarten, S. Calvignac-Spencer, F. H. Leendertz, Investigating the zoonotic origin of the West African Ebola epidemic. *EMBO Molecular Medicine* **7**, 17–23 (2015).

54. A. Mbonye, J. Wamala, W. Kaboyo, V. Tugumizemo, J. Aceng, I. Makumbi, Repeated outbreaks of Viral hemorrhagic fevers in Uganda. *African Health Sciences* **12**, 579–589 (2012).

55. A. A. Dzikwi, I. I. Kuzmin, J. U. Umoh, J. K. P. Kwaga, A. A. Ahmad, C. E. Rupprecht, Evidence of Lagos Bat Virus Circulation among Nigerian Fruit Bats. *Journal of Wildlife Diseases* **46**, 267–271 (2010).

56. M. Sasaki, A. Setiyono, E. Handharyani, I. Rahmadani, S. Taha, S. Adiani, M. Subangkit, H. Sawa, I. Nakamura, T. Kimura, Molecular detection of a novel paramyxovirus in fruit bats from Indonesia. *Virol J* **9**, 240 (2012).

57. M. Alamgir, M. J. Campbell, S. Sloan, A. Suhardiman, J. Supriatna, W. F. Laurance, High-risk infrastructure projects pose imminent threats to forests in Indonesian Borneo. *Sci Rep* **9**, 140 (2019).

58. D. L. A. Gaveau, L. Santos, B. Locatelli, M. A. Salim, H. Husnayaen, E. Meijaard, C. Heatubun, D. Sheil, Forest loss in Indonesian New Guinea (2001–2019): Trends, drivers and outlook. *Biological Conservation* **261**, 109225 (2021).

59. C. L. Faust, H. I. McCallum, L. S. P. Bloomfield, N. L. Gottdenker, T. R. Gillespie, C. J. Torney, A. P. Dobson, R. K. Plowright, Pathogen spillover during land conversion. *Ecology Letters* **21**, 471–483 (2018).

60. F. Keesing, R. D. Holt, R. S. Ostfeld, Effects of species diversity on disease risk. *Ecology Letters* **9**, 485–498 (2006).

61. T. L. Goldberg, T. R. Gillespie, I. B. Rwego, E. L. Estoff, C. A. Chapman, Forest Fragmentation as Cause of Bacterial Transmission among Nonhuman Primates, Humans, and Livestock, Uganda. *Emerg Infect Dis* **14**, 1375–1382 (2008).

62. M. G. Walsh, The Relevance of Forest Fragmentation on the Incidence of Human Babesiosis: Investigating the Landscape Epidemiology of an Emerging Tick-Borne Disease. *Vector-Borne and Zoonotic Diseases* **13**, 250–255 (2013).

63. R. Wilk-da-Silva, P. R. Prist, A. R. Medeiros-Sousa, G. Z. Laporta, L. F. Mucci, M. T. Marrelli, The role of forest fragmentation in yellow fever virus dispersal. *Acta Tropica* **245**, 106983 (2023).

64. F. A. G. de Andrade, M. N. Gomes, W. Uieda, A. L. Begot, O. de S. Ramos, M. E. B. Fernandes, Geographical Analysis for Detecting High-Risk Areas for Bovine/Human Rabies Transmitted by the Common Hematophagous Bat in the Amazon Region, Brazil. *PLOS ONE* **11**, e0157332 (2016).

65. Y. Fan, K. Zhao, Z.-L. Shi, P. Zhou, Bat Coronaviruses in China. *Viruses* **11**, 210 (2019).

66. R. S. Lapuz, A. K. M. Jaojoco, S. R. C. Reyes, J. D. T. D. Alban, K. W. Tomlinson, Greater loss and fragmentation of savannas than forests over the last three decades in Yunnan Province, China. *Environ. Res. Lett.* **17**, 014003 (2021).

67. J. Liu, D. A. Coomes, L. Gibson, G. Hu, J. Liu, Y. Luo, C. Wu, M. Yu, Forest fragmentation in China and its effect on biodiversity. *Biological Reviews* **94**, 1636–1657 (2019).

68. R. M. Beyer, A. Manica, C. Mora, Shifts in global bat diversity suggest a possible role of climate change in the emergence of SARS-CoV-1 and SARS-CoV-2. *Science of The Total Environment* **767**, 145413 (2021).

69. D. J. Becker, P. Eby, W. Madden, A. J. Peel, R. K. Plowright, Ecological conditions predict the intensity of Hendra virus excretion over space and time from bat reservoir hosts. *Ecology Letters* **26**, 23–36 (2023).

70. A. Cimaroli, "Climate Change and Nipah virus: exploring the links between climate variability, extremes, and zoonotic spillover in Bangladesh," thesis, Politecnico di Torino (2024).

71. G. Martin, C. Yanez-Arenas, C. Chen, R. K. Plowright, R. J. Webb, L. F. Skerratt, Climate Change Could Increase the Geographic Extent of Hendra Virus Spillover Risk. *EcoHealth* **15**, 509–525 (2018).

72. P. Eby, Rk. Plowright, H. McCallum, A. Peel, Conditions predict heightened Hendra virus spillover risk in horses this winter: actions now can change outcomes. *Aust Veterinary J* **98**, 270–271 (2020).

73. C. J. Carlson, C. B. Brookson, D. J. Becker, C. A. Cummings, R. Gibb, F. W. Halliday, A. M. Heckley, Z. Y. X. Huang, T. Lavelle, H. Robertson, A. Vicente-Santos, C. M. Weets, T. Poisot, Pathogens and planetary change. *Nat. Rev. Biodivers.* **1**, 32–49 (2025).

74. Y. Liu, R. Liu, L. Qi, J. Chen, J. Dong, X. Wei, Global mapping of fractional tree cover for forest cover change analysis. *ISPRS Journal of Photogrammetry and Remote Sensing* **211**, 67–82 (2024).

75. J. O. Sexton, X.-P. Song, M. Feng, P. Noojipady, A. Anand, C. Huang, D.-H. Kim, K. M. Collins, S. Channan, C. DiMiceli, J. R. Townshend, Global, 30-m resolution continuous fields of tree cover: Landsat-based rescaling of MODIS vegetation continuous fields with lidar-based estimates of error. *International Journal of Digital Earth* **6**, 427–448 (2013).

76. P. G. Murphy, A. E. Lugo, Ecology of Tropical Dry Forest. *Annual Review of Ecology and Systematics* **17**, 67–88 (1986).

77. B. V. Li, A. C. Hughes, C. N. Jenkins, N. Ocampo-Peñuela, S. L. Pimm, Remotely Sensed Data Informs Red List Evaluations and Conservation Priorities in Southeast Asia. *PLOS ONE* **11**, e0160566 (2016).

78. E. Dinerstein, D. Olson, A. Joshi, C. Vynne, N. D. Burgess, E. Wikramanayake, N. Hahn, S. Palminteri, P. Hedao, R. Noss, M. Hansen, H. Locke, E. C. Ellis, B. Jones, C. V. Barber, R. Hayes, C. Kormos, V. Martin, E. Crist, W. Sechrest, L. Price, J. E. M. Baillie, D. Weeden, K. Suckling, C. Davis, N. Sizer, R. Moore, D. Thau, T. Birch, P. Potapov, S. Turubanova, A. Tyukavina, N. de Souza, L. Pintea, J. C. Brito, O. A. Llewellyn, A. G. Miller, A. Patzelt, S. A. Ghazanfar, J. Timberlake, H. Klöser, Y. Shennan-Farpón, R. Kindt, J.-P. B. Lillesø, P. van Breugel, L. Graudal, M. Voge, K. F. Al-Shammari, M. Saleem, An Ecoregion-Based Approach to Protecting Half the Terrestrial Realm. *BioScience* **67**, 534–545 (2017).

79. N. Harris, E. D. Goldman, S. Gibbes, Spatial Database of Planted Trees (SDPT Version 1.0). (2019).

80. T. Sritongchuay, A. C. Hughes, J. Memmott, S. Bumrungsri, Forest proximity and lowland mosaic increase robustness of tropical pollination networks in mixed fruit orchards. *Landscape and Urban Planning* **192**, 103646 (2019).

81. P. Olofsson, G. M. Foody, S. V. Stehman, C. E. Woodcock, Making better use of accuracy data in land change studies: Estimating accuracy and area and quantifying uncertainty using stratified estimation. *Remote Sensing of Environment* **129**, 122–131 (2013).

82. S. J. Phillips, R. P. Anderson, R. E. Schapire, Maximum entropy modeling of species geographic distributions. *Ecological Modelling* **190**, 231–259 (2006).

83. R. G. Pearson, C. J. Raxworthy, M. Nakamura, A. Townsend Peterson, Predicting species distributions from small numbers of occurrence records: a test case using cryptic geckos in

Madagascar: Predicting species distributions with low sample sizes. *Journal of Biogeography* **34**, 102–117 (2006).

84. J. E. Pekar, S. Lytras, M. Ghafari, A. F. Magee, E. Parker, J. L. Havens, A. Katzourakis, T. I. Vasylyeva, M. A. Suchard, A. C. Hughes, J. Hughes, D. L. Robertson, S. Dellicour, M. Worobey, J. O. Wertheim, P. Lemey, The recency and geographical origins of the bat viruses ancestral to SARS-CoV and SARS-CoV-2. *bioRxiv*, 2023.07.12.548617 (2023).

85. GBIF.org, GBIF Occurrence Download, (2023); https://doi.org/10.15468/dl.xc2jvq. 78.

86. GBIF.org, GBIF Occurrence Download, (2022); https://doi.org/10.15468/dl.82sgat.

87. K. C. Tanalgo, J. A. G. Tabora, H. F. M. de Oliveira, D. Haelewaters, C. T. Beranek, A. Otálora-Ardila, E. Bernard, F. Gonçalves, A. Eriksson, M. Donnelly, J. M. González, H. F. Ramos, A. C. Rivas, P. W. Webala, S. Deleva, R. Dalhoumi, J. Maula, D. Lizarro, L. F. Aguirre, N. Bouillard, M. N. R. M. Quibod, J. Barros, M. A. Turcios-Casco, M. Martínez, D. I. Ordoñez-Mazier, J. A. S. Orellana, E. J. Ordoñez-Trejo, D. Ordoñez, A. Chornelia, J. M. Lu, C. Xing, S. Baniya, R. L. Muylaert, L. H. Dias-Silva, N. Ruadreo, A. C. Hughes, DarkCideS 1.0, a global database for bats in karsts and caves. *Sci Data* **9**, 155 (2022).

88. D. N. Karger, O. Conrad, J. Böhner, T. Kawohl, H. Kreft, R. W. Soria-Auza, N. E. Zimmermann, H. P. Linder, M. Kessler, Climatologies at high resolution for the earth's land surface areas. *Scientific Data* **4**, 170122 (2017).

89. R. J. Zomer, J. Xu, A. Trabucco, Version 3 of the Global Aridity Index and Potential Evapotranspiration Database. *Sci Data* **9**, 409 (2022).

90. T. Hengl, J. Mendes de Jesus, G. B. M. Heuvelink, M. Ruiperez Gonzalez, M. Kilibarda, A. Blagotić, W. Shangguan, M. N. Wright, X. Geng, B. Bauer-Marschallinger, M. A. Guevara, R. Vargas, R. A. MacMillan, N. H. Batjes, J. G. B. Leenaars, E. Ribeiro, I. Wheeler, S. Mantel, B. Kempen, SoilGrids250m: Global gridded soil information based on machine learning. *PLoS One* **12**, e0169748 (2017).

91. N. Lang, W. Jetz, K. Schindler, J. D. Wegner, A high-resolution canopy height model of the Earth. *Nat Ecol Evol* **7**, 1778–1789 (2023).

92. K. Didan, MODIS/Terra Vegetation Indices 16-Day L3 Global 1km SIN Grid V061, NASA EOSDIS Land Processes Distributed Active Archive Center (2021); https://doi.org/10.5067/MODIS/MOD13A2.061.

93. D. Yamazaki, D. Ikeshima, J. Sosa, P. D. Bates, G. H. Allen, T. M. Pavelsky, MERIT Hydro: A High-Resolution Global Hydrography Map Based on Latest Topography Dataset. *Water Resources Research* **55**, 5053–5073 (2019).

94. J. M. Kass, R. Muscarella, P. J. Galante, C. L. Bohl, G. E. Pinilla-Buitrago, R. A. Boria, M. Soley-Guardia, R. P. Anderson, ENMeval 2.0: Redesigned for customizable and reproducible modeling of species' niches and distributions. *Methods in Ecology and Evolution* **12**, 1602–1608 (2021).

95. O. Allouche, A. Tsoar, R. Kadmon, Assessing the accuracy of species distribution models: prevalence, kappa and the true skill statistic (TSS). *Journal of Applied Ecology* **43**, 1223–1232 (2006).

96. IUCN, Digital Distribution Maps on The IUCN Red List of Threatened Species. Version 6.3., (2022); https://www.iucnredlist.org.

97. W. F. Laurance, M. Goosem, S. G. W. Laurance, Impacts of roads and linear clearings on tropical forests. *Trends in Ecology & Evolution* **24**, 659–669 (2009).

Acknowledgments

The computations were performed using research computing facilities offered by Information Technology Services, the University of Hong Kong.

Author contributions:

Conceptualization: RSL, ACH
Methodology: RSL, ACH
Formal analysis: RSL
Data curation: RSL, ACH, AC
Visualization: RSL
Supervision: ACH
Writing—original draft: RSL
Writing—review & editing: RSL, ACH

Competing interests: Authors declare that they have no competing interests.

Data and materials availability: All data are available in the main text or the supplementary materials.

Science Advances
AAAS

Supplementary Materials for

Mapping the potential risk of coronavirus spillovers in South and Southeast Asia

R. Sedricke Lapuz *et al.*

*Corresponding author. Email: achughes@hku.hk; alice.c.hughes@unimelb.edu.au

This PDF file includes:

Supplementary Text

Fragmentation results

Analyses of fragmentation in the baseline forest cover map revealed differences for each country/territory (Supplementary Table S2). Bhutan and Papua New Guinea had the most intact forests, as indicated by having the fewest forest patches, but with the highest forest patch index and mean patch area values and high patch cohesion indices, signifying the presence of a large, continuous forest with high connectivity. Taiwan, Brunei, and Nepal followed suit. In contrast, China had the most forest patches and the highest edge length values, indicating extensive forest edge exposure. Relative to its land area, it also had low mean patch area and high patch index values. These collectively suggest that China has the most fragmented forest in our study region. Indonesia had high mean patch area and LPI values due to the intact forest cover in Borneo and Sulawesi, but also had the second highest number of forest patches, implying that a lot of fragmentation has occurred in the other major islands of Sumatra and Java.

Introducing road networks over the habitat increased fragmentation generally across all countries (Supplementary Table S2). All countries/territories experienced a decrease in mean patch area and patch cohesion index values, and all except Bangladesh had a decline in their largest patch index values. The most dramatic change is from Papua New Guinea, which experienced a +335.1% increase in number of patches concurrently with a -83.1% decrease in mean patch area and a -48.9% decline in its largest patch index value.

Forest cover and species distribution modeling results

The resulting forest cover map showed that in mainland Asia, most of the forest cover retained are on the mountainous areas, from the Himalayas in the Indian subcontinent, extending eastward to the mountains over Myanmar and western China, and down to the mountains of Indochina and peninsular southeast Asia. Forest cover across southern China exhibited a patchier appearance. In the islands, New Guinea, Borneo, and Sulawesi are mostly still covered by large

swaths of forest, while Sumatra, Java, and the Philippines are only forested in their montane regions.

Upon combining the predicted maps, we found that the Rhinolophid bat habitats were concentrated in the Indochina region, with the highest species richness numbers seen in Thailand, Laos, Cambodia, and Vietnam, while also extending slightly northwards to Yunnan and Guangxi provinces in southwest China (Figure S1). Northern Myanmar, eastern Himalaya, peninsular Malaysia, and the rest of southern China had moderate species richness numbers, while Borneo, Sumatra and Philippines were seen to have low Rhinolophid bat species richness. Finally, most of the Indian subcontinent and New Guinea had the lowest richness.

All species distribution models yielded good scores. Mean AUC score was at 0.861, ranging 0.780 to 0.951, while TSS scores had a mean of 0.534 and ranging from 0.278 to 0.875 (see Table S3), allowing all models to be predicted to space and used for further analyses. With regards to the percent contribution of the predictors, temperature annual range (Bio7) and mean canopy height registered as the highest-ranking predictors across most of the bat SDMs, while precipitation seasonality (Bio15) and mean annual temperature (Bio1) mostly ranked second (Supp Table 2). These suggest that climatic variables and vegetation cover mostly dictate the spaces which the Rhinolophid bats find to be most suitable.

Table S1. Accuracy metrics for forest cover map

Land cover class	Area (km²)	Area uncertainty (km²±)	PA	PA±	UA	UA±	OA	OA±
Non forest	2,184,034.7	51,503.22	97.3	0.74	98	2.25	96.06	1.98
Tropical moist forest	293,553.35	42,548.39	90.15	12.27	89.33	4.96		
Tropical dry forest	13,668.14	784.64	100	0	88.67	5.09		
Temperate forest	105,579.04	29,379.43	86.31	23.18	78	6.65		

Legend: PA – Producer's Accuracy; UA – User's Accuracy; OA – Overall Accuracy

Data S1. List of sources of infrastructure shapefiles used for analyses

1. OpenStreetMap (https://download.geofabrik.de/; downloaded on 23 March 2024)
2. Data from: Trans-National Conservation and Infrastructure Development in The Heart of Borneo. Published Nov 26, 2019 on Dryad. https://doi.org/10.5061/dryad.s4m5q53.
3. Data from: Infrastructure expansion challenges sustainable development in Papua New Guinea. Published Jul 30, 2019 on Dryad. https://doi.org/10.5061/dryad.3p84s7s
4. Data from: Satellite images and road-reference data for AI-based road mapping in Equatorial Asia. Published Sep 18, 2023; Updated Apr 04, 2024 on Dryad. https://doi.org/10.5061/dryad.bvq83bkg7
5. Emerging challenges for sustainable development and forest conservation in Sarawak, Borneo. Published Aug 16, 2020 on Dryad. https://doi.org/10.5061/dryad.547d7wm4v
6. Indonesian road network: https://www.indonesia-geospasial.com/2020/12/download-shp-jaringan-jalan.html.html
7. Indian map of proposed highways: https://www.google.com/maps/d/u/0/viewer?msa=0&mid=1tUXlNp9QD1PE9pjDzbQMJaY9cvE&ll=23.199425243350444%2C79.36049818164062&z=6
8. Man, Chun Yin; Palmer, David Alexander (2022). Geo-mapping databases of the Belt and Road Initiative. figshare. Collection. https://doi.org/10.6084/m9.figshare.c.6076193
9. Griffiths, Richard & Hughes, Alice. (2021). In the Way of the Road. The Ecological Consequences of Infrastructure. Publisher: International Institute for Asian Studies.

Table S2. Fragmentation metrics for two scenarios for each country

Country/Territory	Number of Patches			Mean Patch Area (ha)			Largest Patch Index (%)		
	BL	BL + NI	% Change	BL	BL + NI	% Change	BL	BL + NI	% Change
Afghanistan	214	183	-14.5	1865.89	1977.60	6.0	0.45	0.40	-11.7
Bangladesh	556	485	-12.8	1062.95	1156.49	8.8	0.60	0.61	1.3
Bhutan	113	89	-21.2	34470.80	33753.93	-2.1	76.78	58.69	-23.6
Brunei	32	40	25.0	14259.38	10152.50	-28.8	56.79	51.00	-10.2
Cambodia	679	619	-8.8	6961.12	7495.80	7.7	8.49	7.48	-11.8
China	29981	32541	8.5	3207.39	2188.37	-31.8	4.57	0.22	-95.1
East Timor	241	247	2.5	1793.78	1548.18	-13.7	13.92	9.78	-29.8
India	7565	8498	12.3	4823.94	3225.72	-33.1	4.73	1.97	-58.4
Indonesia	10522	11930	13.4	10418.19	7638.63	-26.7	18.30	12.80	-30.0
Laos	1815	1916	5.6	7373.28	6749.53	-8.5	38.72	9.05	-76.6
Malaysia	2033	1805	-11.2	9697.88	9298.56	-4.1	38.75	23.98	-38.1
Myanmar	3268	3482	6.5	10727.42	9637.62	-10.2	20.78	17.16	-17.4
Nepal	1169	1250	6.9	7240.72	5506.40	-24.0	42.17	9.81	-76.7
Pakistan	1171	979	-16.4	2083.69	2042.19	-2.0	1.29	0.62	-52.0
Papua New Guinea	649	2824	335.1	63042.53	10675.96	-83.1	74.69	38.19	-48.9
Philippines	2409	2844	18.1	5212.20	3229.22	-38.0	9.71	2.82	-70.9
Singapore	16	7	-56.3	700.00	428.57	-38.8	14.29	2.66	-81.4
Sri Lanka	322	463	43.8	2022.98	905.40	-55.2	7.89	0.95	-87.9
Taiwan	117	272	132.5	21194.87	7771.32	-63.3	53.74	37.28	-30.6
Thailand	2221	2318	4.4	5389.10	4532.70	-15.9	5.25	2.56	-51.2
Vietnam	2393	2720	13.7	4277.31	3297.50	-22.9	5.44	1.43	-73.7

Note: BL – Baseline; BL + NI – Baseline + New Infrastructure

Table S2 (con't)

Country/Territory	Mean Shape Index			Total Edge Length (m)		
	BL	BL + NI	% Change	BL	BL + NI	% Change
Afghanistan	1.33	1.36	2.0	4.77E+06	4.35E+06	-8.6
Bangladesh	1.24	1.26	0.9	8.89E+06	8.14E+06	-8.5
Bhutan	1.18	1.41	19.9	8.53E+06	1.14E+07	33.9
Brunei	1.40	1.37	-1.8	1.53E+06	1.63E+06	6.3
Cambodia	1.25	1.30	4.0	2.31E+07	2.25E+07	-2.8
China	1.31	1.36	4.1	8.90E+08	7.71E+08	-13.4
East Timor	1.33	1.35	1.0	5.75E+06	5.28E+06	-8.1
India	1.25	1.33	6.1	2.40E+08	2.32E+08	-3.2
Indonesia	1.26	1.30	2.8	3.72E+08	4.22E+08	13.5
Laos	1.28	1.34	4.8	7.98E+07	7.95E+07	-0.4
Malaysia	1.25	1.33	6.1	6.99E+07	6.70E+07	-4.1
Myanmar	1.28	1.35	5.7	1.61E+08	1.68E+08	3.8
Nepal	1.23	1.42	15.2	6.55E+07	6.02E+07	-8.1
Pakistan	1.26	1.31	4.0	2.58E+07	2.23E+07	-13.7
Papua New Guinea	1.25	1.31	5.2	7.55E+07	1.28E+08	70.2
Philippines	1.31	1.27	-2.3	8.22E+07	6.63E+07	-19.4
Singapore	1.27	1.16	-9.1	1.98E+05	6.40E+04	-67.7
Sri Lanka	1.26	1.26	0.2	7.94E+06	6.59E+06	-17.0
Taiwan	1.35	1.31	-2.7	7.88E+06	9.06E+06	14.9
Thailand	1.30	1.36	4.7	7.76E+07	7.48E+07	-3.6
Vietnam	1.30	1.34	2.7	7.56E+07	7.26E+07	-3.9

Note: BL – Baseline; BL + NI – Baseline + New Infrastructure

Table S2 (con't)

Country/Territory	Edge density (m/ha)			Patch cohesion index (%)		
	BL	BL + NI	% Change	BL	BL + NI	% Change
Afghanistan	0.16	0.15	-3.3	93.76	93.33	-0.5
Bangladesh	0.55	0.53	-4.0	92.47	92.08	-0.4
Bhutan	1.69	2.39	41.4	99.89	99.76	-0.1
Brunei	2.70	2.97	10.0	98.65	98.24	-0.4
Cambodia	1.22	1.20	-1.0	98.84	98.37	-0.5
China	1.40	1.25	-11.1	99.26	94.57	-4.7
East Timor	3.75	3.60	-3.9	96.27	93.91	-2.4
India	0.64	0.63	-1.0	99.49	98.05	-1.4
Indonesia	1.99	2.32	16.6	99.66	99.52	-0.1
Laos	3.14	3.15	0.2	99.66	98.57	-1.1
Malaysia	2.13	2.08	-2.5	99.66	99.22	-0.4
Myanmar	2.12	2.22	5.1	99.60	99.26	-0.3
Nepal	3.46	3.34	-3.6	99.80	98.65	-1.2
Pakistan	0.29	0.26	-10.4	97.93	96.42	-1.5
Papua New Guinea	1.61	2.81	74.7	99.94	99.66	-0.3
Philippines	2.71	2.32	-14.5	98.74	96.28	-2.5
Singapore	4.10	1.42	-65.4	81.99	61.54	-24.9
Sri Lanka	1.19	1.02	-14.4	98.20	87.43	-11.0
Taiwan	1.84	2.16	17.4	99.63	98.82	-0.8
Thailand	1.40	1.38	-1.7	98.78	96.89	-1.9
Vietnam	2.10	2.05	-2.3	98.46	95.69	-2.8

Note: BL – Baseline scenario; BL + NI – Baseline + New Infrastructure scenario

Table S3. Parameters used and accuracy metrics for Maxent species models

Species	TPT	FC	RM	Training AUC	TSS
Rhinolophus acuminatus	0.1752	LQH	3	0.873	0.500
Rhinolophus affinis	0.3038	LQH	1	0.839	0.517
Rhinolophus arcuatus	0.1221	LQ	1	0.866	0.480
Rhinolophus beddomei	0.3021	LQ	1	0.960	0.786
Rhinolophus borneensis	0.2698	LQ	1	0.803	0.420
Rhinolophus celebensis	0.0747	LQ	1	0.870	0.366
Rhinolophus chaseni	0.2692	LQ	1	0.905	0.686
Rhinolophus coelophyllus	0.3131	LQH	5	0.836	0.492
Rhinolophus cornutus	0.1923	LQ	1	0.840	0.376
Rhinolophus euryotis	0.4897	LQH	2	0.793	0.412
Rhinolophus ferrumequinum	0.2319	LQ	1	0.896	0.627
Rhinolophus formosae	0.3471	LQ	1	0.949	0.788
Rhinolophus indorouxii	0.3965	LQ	3	0.964	0.775
Rhinolophus inops	0.2549	LQ	4	0.780	0.278
Rhinolophus lepidus	0.1465	LQH	3	0.891	0.568
Rhinolophus luctus	0.3039	LQH	3	0.825	0.455
Rhinolophus macrotis	0.3633	LQ	1	0.812	0.487
Rhinolophus malayanus	0.346	H	3	0.817	0.453
Rhinolophus marshalli	0.2884	LQ	1	0.830	0.425
Rhinolophus megaphyllus	0.1049	LQ	1	0.885	0.411
Rhinolophus microglobosus	0.2553	LQ	1	0.848	0.517
Rhinolophus monoceros	0.4048	H	5	0.951	0.875
Rhinolophus pearsonii	0.3028	H	2	0.876	0.577
Rhinolophus philippinensis	0.3864	LQH	4	0.841	0.509
Rhinolophus pusillus	0.3673	LQH	2	0.820	0.504
Rhinolophus refulgens	0.4239	LQ	2	0.882	0.552
Rhinolophus rex	0.334	LQ	1	0.786	0.384
Rhinolophus robinsoni	0.1898	LQ	2	0.908	0.669
Rhinolophus rouxii	0.2701	LQH	1	0.876	0.604
Rhinolophus rufus	0.6113	LQH	5	0.825	0.500
Rhinolophus sedulus	0.2673	LQH	3	0.917	0.737
Rhinolophus shameli	0.2848	LQH	4	0.876	0.592
Rhinolophus siamensis	0.4087	LQH	1	0.800	0.430
Rhinolophus sinicus	0.4028	LQH	3	0.867	0.605
Rhinolophus stheno	0.2165	LQH	3	0.860	0.514
Rhinolophus subbadius	0.4034	LQH	4	0.956	0.736
Rhinolophus subrufus	0.3611	L	5	0.780	0.399
Rhinolophus tatar	0.112	LQH	4	0.956	0.652
Rhinolophus thomasi	0.2929	H	5	0.833	0.374
Rhinolophus trifoliatus	0.2196	LQH	3	0.896	0.622

Rhinolophus virgo	0.2258	LQ	1	0.814	0.381
Rhinolophus yunanensis	0.4731	LQH	3	0.777	0.400

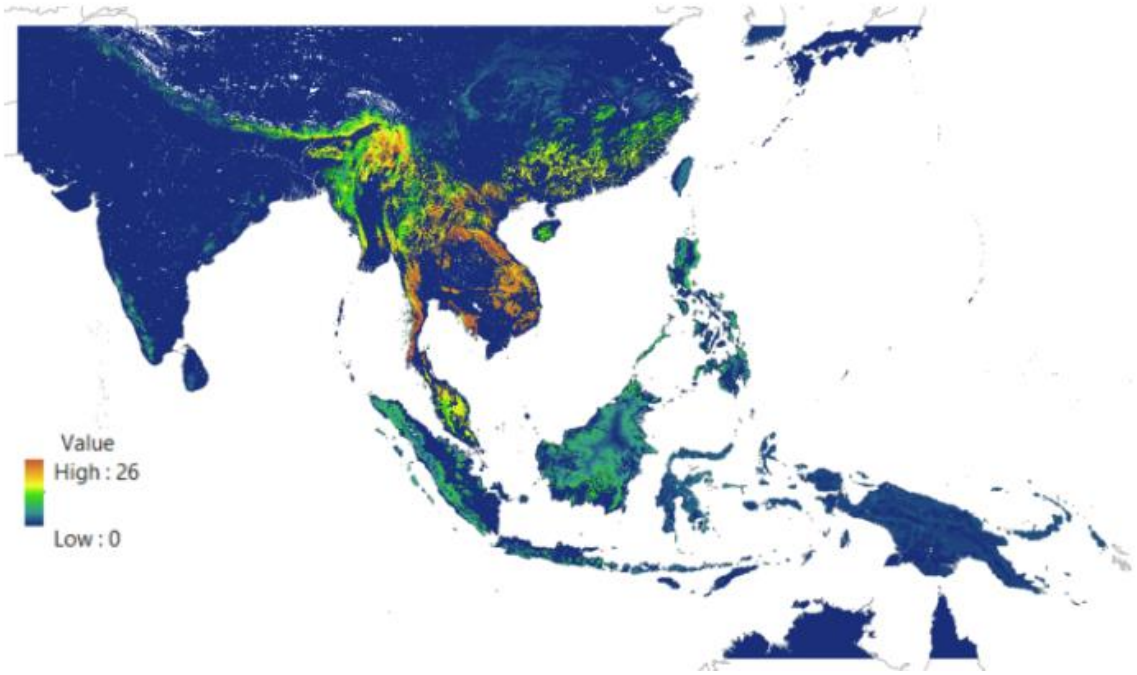

Figure S1. Map of tropical east Asia showing Rhinolophid species richness based on species distribution models

Data S2. List of additional species occurrence points sources

- Bergmans, W., & Rozendaal, F. G. (1982). Notes on Rhinolophus Lacépède, 1799 from Sulawesi, Indonesia, with the description of a new species (Mammalia, Microchiroptera). Bijdragen tot de Dierkunde, 52(2), 169-174.
- Bergmans, W., & Rozendaal, F. G. (1982). Notes on Rhinolophus Lacépède, 1799 from Sulawesi, Indonesia, with the description of a new species (Mammalia, Microchiroptera). Bijdragen tot de Dierkunde, 52(2), 169-174.
- Ith, S., Bumrungsri, S., Furey, N. M., Bates, P. J., Wonglapsuwan, M., Khan, F. A. A., ... & Thomas, N. M. (2015). Taxonomic implications of geographical variation in *Rhinolophus affinis* (Chiroptera: Rhinolophidae) in mainland Southeast Asia. Zoological Studies, 54, 1-29. Kartono AP, Prayogi KD, Maryanto I. (2017). Keanekaragaman jenis kelelawar di Hutan Pendidikan Gunung Walat Sukabumi Jawa Barat. Zoo Indonesia. 26(1):33-43
- Kitchener, D. J., Schmitt, L. H., Strano, P., Wheeler, A., & Suyanto, A. (1995). Taxonomy of *Rhinolophus simplex* Andersen, 1905 (Chiroptera: Rhinolophidae) in Nusa Tenggara and Maluku, Indonesia. Records of the Western Australian Museum, 17, 1-28.
- Kruskop, S.V., Eger, J.L., Lim, B.K., Engstrom, M.D., Francis, C.M., Guillen Servent, A., Ivanova, N.V. and Borisenko, A.V. Bats of Southeast Asia, Part 2.
- Maharadatunkamsi, Hisheh, S., Kitchener, D. J., & Schmitt, L. H. (2000). Genetic and morphometric diversity in Wallacea: geographical patterning in the horse shoe bat, *Rhinolophus affinis.* Journal of Biogeography, 27(1), 193-201.
- Nurfitrianto H, Budijastuti W, Faizah U. (2013). Kekayaan jenis kelelawar (Chiroptera) di kawasan gua Lawa Karst Dander Kabupaten Bojonegoro. LenteraBio. 2(2): 143-151
- Patterson, G., Martin, T. E., Adams, N., Cropper, O., Mustari, A. H., & Tosh, D. G. (2017). Lowland rainforest bat communities of Buton Island, Southeast Sulawesi, including new regional records. Raffles Bulletin of Zoology, 65.

Table S4. Relative eRIDE, Relative Population at Risk, and Relative Pandemic Risk scores for each country

COUNTRY	ISO3 CODE	eRIDE INDEX			POPULATION AT RISK (PAR) SCORE			Pandemic Risk		
		BL	BL+NI	Change	BL	BL+NI	Change	BL	BL+NI	Change
Afghanistan	AFG	0.0	0.0	0.0	0.0	0.0	0.0	1.0	1.0	0.0
Bangladesh	BGD	0.3	0.3	0.0	0.6	0.7	0.1	5.5	8.0	2.5
Bhutan	BTN	0.7	1.0	0.3	0.5	0.7	0.3	0.2	0.2	0.0
Brunei	BRN	0.1	0.1	0.0	0.0	0.0	0.0	0.0	0.0	0.0
Cambodia	KHM	2.9	3.1	0.2	0.4	0.6	0.2	0.7	0.2	-0.5
China	CHN	24.8	22.0	-2.8	29.6	27.8	-1.8	30.0	16.7	-13.3
East Timor	TLS	0.0	0.0	0.0	0.0	0.0	0.0	0.0	0.0	0.0
India	IND	9.9	9.9	0.0	21.2	20.9	-0.3	47.0	62.0	15.0
Indonesia	IDN	10.0	11.1	1.1	13.5	14.1	0.6	0.7	0.5	-0.2
Laos	LAO	10.7	11.1	0.4	2.3	2.7	0.4	0.9	0.2	-0.7
Malaysia	MYS	3.3	3.5	0.2	2.0	1.6	-0.4	0.6	0.2	-0.4
Myanmar	MMR	16.5	17.5	0.9	5.3	6.9	1.6	2.7	2.2	-0.5
Nepal	NPL	2.3	2.1	-0.2	6.1	6.3	0.2	0.8	0.8	0.0
Pakistan	PAK	0.4	0.3	-0.1	2.7	2.5	-0.1	5.4	6.3	0.9
Papua New Guinea	PNG	1.1	1.2	0.1	0.5	0.6	0.1	0.0	0.0	0.0
Philippines	PHL	2.2	2.2	0.0	3.0	2.9	-0.1	0.3	0.1	-0.2
Singapore	SGP	0.0	0.0	0.0	0.0	0.0	0.0	0.0	0.0	0.0
Sri Lanka	LKA	0.1	0.1	0.0	0.7	0.3	-0.3	0.0	0.0	0.0
Taiwan	TWN	0.2	0.2	0.0	0.5	0.2	-0.3	0.0	0.0	0.0
Thailand	THA	7.1	7.2	0.1	3.0	3.7	0.6	2.3	0.8	-1.5
Vietnam	VNM	7.3	7.0	-0.3	6.3	7.0	0.6	1.8	0.7	-1.0

Note: BL – Baseline scenario; BL + NI – Baseline + New Infrastructure scenario

Table S5. Percentage of eRIDE risk areas categorized by eRIDE values for each country under baseline (BL) and new infrastructure (NI) scenarios. Risk level categories are determined by the geometric intervals of the eRIDE values. Cells are color-coded to represent the percentage of coverage for each risk category, indicating the respective country's risk level in each scenario.

Country	Risk Level Category Percentages									
	Low		Moderately Low		High		Moderately High		Highest	
	BL	NI	BL	NI	BL	NI	BL	NI	BL	NI
Afghanistan	10.2	10.0	68.4	68.7	21.5	21.2	0.0	0.0	0.0	0.0
Bangladesh	2.5	2.4	4.4	3.7	16.0	17.9	70.9	69.8	6.2	6.1
Bhutan	3.9	1.8	24.2	15.3	47.0	36.6	24.3	41.3	0.7	4.9
Brunei Darussalam	8.4	9.0	23.4	17.3	52.6	52.8	15.6	20.9	0.0	0.0
Cambodia	0.7	0.7	3.4	3.4	12.6	12.2	47.7	45.5	35.6	38.2
China	5.8	3.9	33.5	35.3	22.9	23.3	25.9	27.2	12.0	10.3
India	3.3	3.1	17.9	17.1	28.9	26.9	42.5	45.0	7.4	8.0
Indonesia	21.6	15.8	39.2	41.5	28.4	31.4	10.8	11.3	0.0	0.0
Laos	0.2	0.2	1.1	1.0	5.0	4.4	37.1	36.5	56.5	57.8
Malaysia	12.6	10.2	18.8	19.2	37.1	38.7	30.4	30.8	1.0	1.0
Myanmar	1.7	1.6	8.0	7.4	16.4	15.2	52.5	54.4	21.4	21.4
Nepal	0.9	1.0	23.6	24.7	33.9	35.4	34.0	32.7	7.6	6.1
Pakistan	4.9	5.6	35.0	37.0	47.2	48.0	13.0	9.4	0.0	0.0
Papua New Guinea	43.2	36.7	55.1	61.1	1.7	2.2	0.0	0.0	0.0	0.0
Philippines	2.8	1.8	12.0	10.8	58.0	60.8	27.2	26.6	0.0	0.0
Singapore	44.7	100.0	55.3	0.0	0.0	0.0	0.0	0.0	0.0	0.0
Sri Lanka	3.1	5.8	16.9	22.3	79.9	71.8	0.2	0.0	0.0	0.0
Taiwan	5.5	2.9	49.9	41.2	44.6	56.0	0.0	0.0	0.0	0.0
Thailand	0.4	0.4	1.7	1.8	7.0	6.8	52.5	53.1	38.3	37.9
Timor-Leste	6.7	8.1	80.3	80.3	13.0	11.7	0.0	0.0	0.0	0.0
Viet Nam	0.2	0.2	0.9	0.9	4.9	4.2	42.7	42.8	51.3	52.0

Table S6. Percentage of population-at-risk (PAR) areas categorized by PAR values for each country under baseline (BL) and new infrastructure (NI) scenarios. Risk level categories are determined by the geometric intervals of the PAR values. Cells are color-coded to represent the percentage of coverage for each risk category, indicating the respective country's risk level in each scenario.

Country	Risk Level Category Percentages									
	Low		Moderately Low		High		Moderately High		Highest	
	BL	NI	BL	NI	BL	NI	BL	NI	BL	NI
Afghanistan	0.0	0.0	0.6	0.6	2.8	2.9	95.0	94.9	1.7	1.6
Bangladesh	0.0	0.0	0.0	0.0	0.0	0.0	24.9	26.5	75.1	73.4
Bhutan	0.3	0.3	8.5	7.0	17.1	14.1	61.0	60.3	13.2	18.3
Brunei Darussalam	20.3	18.5	35.9	38.8	14.4	16.4	21.0	21.9	8.4	4.3
Cambodia	0.2	0.2	10.3	10.0	12.6	12.5	68.0	68.4	8.9	9.0
China	0.1	0.1	4.0	3.4	7.7	7.9	51.8	55.2	36.5	33.4
India	0.7	0.7	5.2	4.9	6.5	6.5	41.0	43.6	46.5	44.2
Indonesia	1.3	1.1	19.8	19.1	19.1	19.5	48.4	50.1	11.5	10.1
Laos	0.3	0.3	4.9	4.5	10.2	10.4	68.1	69.7	16.5	15.1
Malaysia	3.5	2.6	20.6	22.3	16.4	16.8	52.3	53.0	7.2	5.3
Myanmar	0.4	0.4	7.2	6.9	7.7	7.8	64.0	65.2	20.7	19.8
Nepal	0.0	0.0	1.2	1.3	3.6	3.9	40.4	43.4	54.8	51.4
Pakistan	0.0	0.0	0.3	0.3	1.2	1.4	32.7	35.3	65.8	63.0
Papua New Guinea	1.3	1.2	41.5	39.8	30.3	30.2	26.1	28.3	0.8	0.6
Philippines	0.0	0.0	4.1	3.4	8.2	8.2	61.1	65.6	26.6	22.8
Singapore	0.0	0.0	0.0	0.0	0.0	6.7	13.9	53.3	86.1	40.0
Sri Lanka	0.1	0.1	0.4	0.8	1.3	1.9	16.0	27.1	82.2	70.1
Taiwan	0.1	0.1	19.6	16.1	31.3	37.2	39.9	42.2	9.1	4.4
Thailand	0.0	0.0	0.4	0.5	1.7	1.8	54.5	56.2	43.3	41.6
Timor-Leste	0.0	0.0	0.5	0.7	17.5	20.2	74.3	74.1	7.7	5.0
Viet Nam	0.0	0.0	0.0	0.0	0.3	0.2	23.6	23.4	76.0	76.4

Table S7. Percentage of pandemic spread risk areas categorized by pandemic spread risk values for each country under baseline (BL) and new infrastructure (NI) scenarios. Risk level categories are determined by the geometric intervals of the pandemic spread risk values. Cells are color-coded to represent the percentage of coverage for each risk category, indicating the respective country's risk level in each scenario.

	Risk Level Category Percentages									
Country	**Low**		**Moderately Low**		**High**		**Moderately High**		**Highest**	
	BL	**NI**	**BL**	**NI**	**BL**	**NI**	**BL**	**NI**	**BL**	**NI**
Afghanistan	99.90	99.90	0.03	0.03	0.03	0.00	0.03	0.07	0.00	0.00
Bangladesh	38.31	34.51	5.10	4.42	26.06	20.77	30.35	40.17	0.19	0.12
Bhutan	100.00	100.00	0.00	0.00	0.00	0.00	0.00	0.00	0.00	0.00
Brunei Darussalam	100.00	100.00	0.00	0.00	0.00	0.00	0.00	0.00	0.00	0.00
Cambodia	99.89	100.00	0.11	0.00	0.00	0.00	0.00	0.00	0.00	0.00
China	97.32	99.38	1.45	0.22	0.98	0.25	0.25	0.15	0.01	0.01
India	88.94	85.63	3.51	4.04	5.54	7.13	1.98	3.16	0.03	0.04
Indonesia	99.88	99.92	0.01	0.01	0.06	0.04	0.05	0.03	0.00	0.00
Laos	100.00	100.00	0.00	0.00	0.00	0.00	0.00	0.00	0.00	0.00
Malaysia	99.82	99.85	0.00	0.00	0.09	0.06	0.09	0.09	0.00	0.00
Myanmar	99.95	99.96	0.01	0.00	0.03	0.00	0.01	0.04	0.00	0.00
Nepal	99.58	99.42	0.00	0.05	0.21	0.27	0.16	0.27	0.05	0.00
Pakistan	97.01	95.72	1.43	1.48	1.28	2.44	0.25	0.32	0.03	0.03
Papua New Guinea	100.00	100.00	0.00	0.00	0.00	0.00	0.00	0.00	0.00	0.00
Philippines	99.84	99.87	0.00	0.03	0.10	0.07	0.06	0.03	0.00	0.00
Singapore	100.00	100.00	0.00	0.00	0.00	0.00	0.00	0.00	0.00	0.00
Sri Lanka	100.00	100.00	0.00	0.00	0.00	0.00	0.00	0.00	0.00	0.00
Taiwan	100.00	100.00	0.00	0.00	0.00	0.00	0.00	0.00	0.00	0.00
Thailand	99.58	99.74	0.09	0.02	0.13	0.07	0.18	0.16	0.02	0.00
Timor-Leste	100.00	100.00	0.00	0.00	0.00	0.00	0.00	0.00	0.00	0.00
Viet Nam	98.76	99.55	0.65	0.20	0.37	0.11	0.20	0.11	0.03	0.03

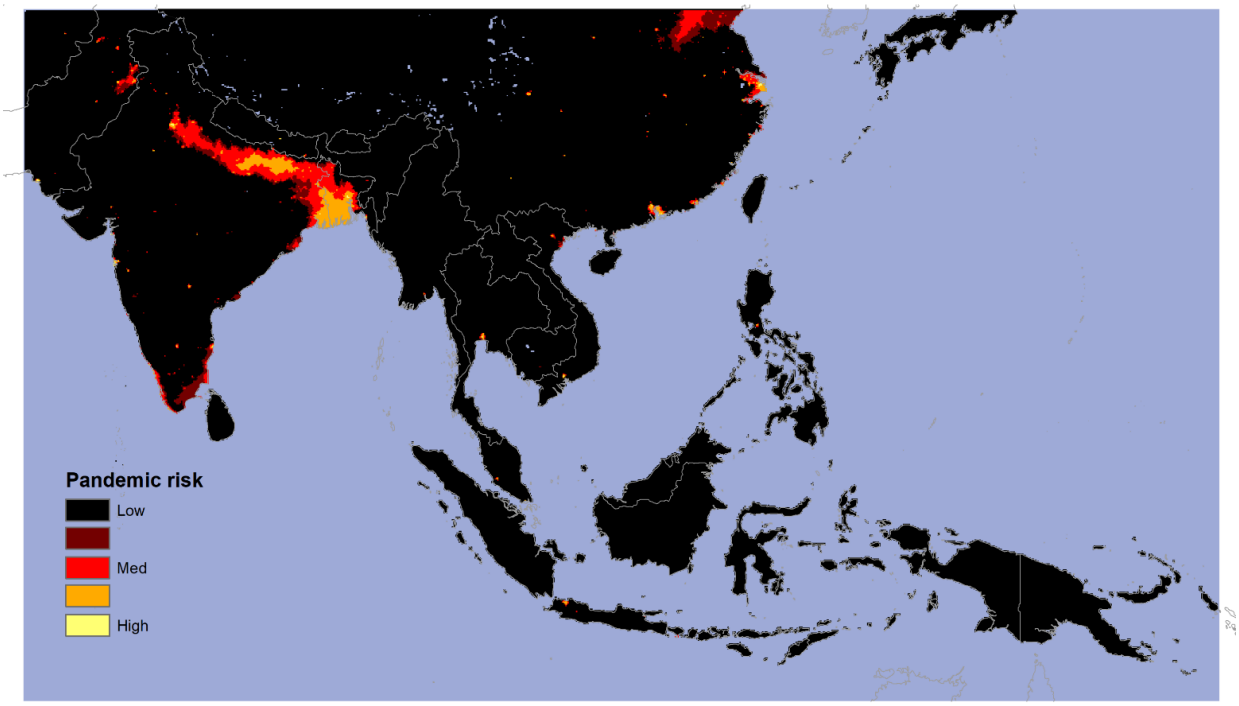

Figure S2. Map of pandemic spread risk in tropical east Asia under baseline + new infrastructure scenario

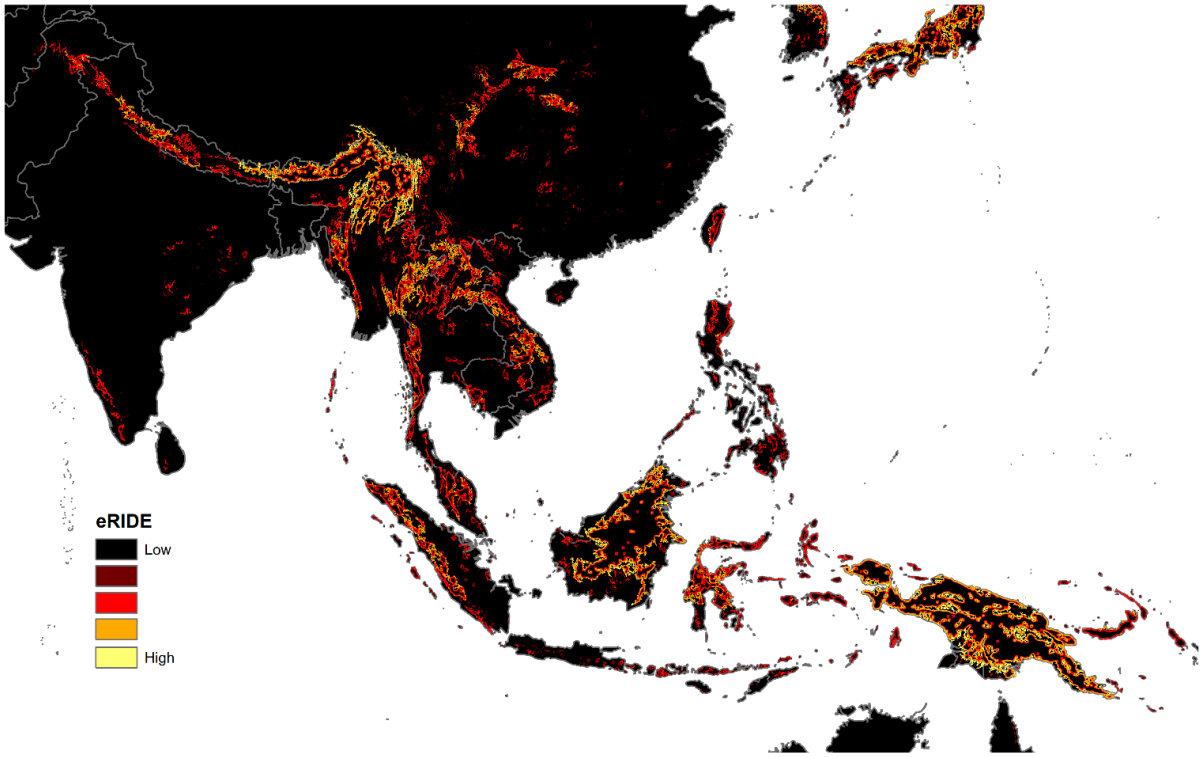

Figure S3. Map of tropical east Asia depicting eRIDE hotspots using the species-area relationship to estimate biodiversity values within each forest patch.

Table S8. Percentage of risk areas for each country categorized using eRIDE values under baseline (BL) and new infrastructure scenarios (BL + NI), with scenario comparison

Country	*Low Risk*			*Moderately Low Risk*			*High Risk*			*Moderately High Risk*			*Highest Risk*		
	BL	**BL+NI**	**Change**	**BL**	**BL+NI**	**Change**	**BL**	**BL+NI**	**Change**	**BL**	**BL+NI**	**Change**	**BL**	**BL+NI**	**Change**
Afghanistan	10.2	10.0	0.1	68.4	68.7	0.4	21.5	21.2	-0.2	0.0	0.0	0.0	0.0	0.0	0.0
Bangladesh	2.5	2.4	0.1	4.4	3.7	-0.7	16.0	17.9	2.0	70.9	69.8	-1.1	6.2	6.1	-0.1
Bhutan	3.9	1.8	2.1	24.2	15.3	-8.8	47.0	36.6	-10.3	24.3	41.3	17.0	0.7	4.9	4.2
Brunei Darussalam	8.4	9.0	-0.6	23.4	17.3	-6.0	52.6	52.8	0.2	15.6	20.9	5.2	0.0	0.0	0.0
Cambodia	0.7	0.7	0.0	3.4	3.4	0.0	12.6	12.2	-0.4	47.7	45.5	-2.2	35.6	38.2	2.6
China	5.8	3.9	1.9	33.5	35.3	1.8	22.9	23.3	0.4	25.9	27.2	1.4	12.0	10.3	-1.7
India	3.3	3.1	0.2	17.9	17.1	-0.9	28.9	26.9	-2.0	42.5	45.0	2.5	7.4	8.0	0.6
Indonesia	21.6	15.8	5.8	39.2	41.5	2.3	28.4	31.4	3.0	10.8	11.3	0.5	0.0	0.0	0.0
Laos	0.2	0.2	0.0	1.1	1.0	-0.1	5.0	4.4	-0.6	37.1	36.5	-0.6	56.5	57.8	1.3
Malaysia	12.6	10.2	2.4	18.8	19.2	0.4	37.1	38.7	1.6	30.4	30.8	0.4	1.0	1.0	0.0
Myanmar	1.7	1.6	0.1	8.0	7.4	-0.5	16.4	15.2	-1.2	52.5	54.4	1.8	21.4	21.4	0.0
Nepal	0.9	1.0	0.0	23.6	24.7	1.2	33.9	35.4	1.5	34.0	32.7	-1.2	7.6	6.1	-1.5
Pakistan	4.9	5.6	-0.8	35.0	37.0	2.0	47.2	48.0	0.8	13.0	9.4	-3.6	0.0	0.0	0.0
Papua New Guinea	43.2	36.7	6.5	55.1	61.1	6.0	1.7	2.2	0.6	0.0	0.0	0.0	0.0	0.0	0.0
Philippines	2.8	1.8	1.0	12.0	10.8	-1.2	58.0	60.8	2.8	27.2	26.6	-0.6	0.0	0.0	0.0
Sri Lanka	3.1	5.8	-2.8	16.9	22.3	5.5	79.9	71.8	-8.1	0.2	0.0	-0.2	0.0	0.0	0.0
Taiwan	5.5	2.9	2.7	49.9	41.2	-8.7	44.6	56.0	11.4	0.0	0.0	0.0	0.0	0.0	0.0
Thailand	0.4	0.4	0.0	1.7	1.8	0.1	7.0	6.8	-0.2	52.5	53.1	0.6	38.3	37.9	-0.4
Timor-Leste	6.7	8.1	-1.4	80.3	80.3	0.0	13.0	11.7	-1.4	0.0	0.0	0.0	0.0	0.0	0.0
Viet Nam	0.2	0.2	0.0	0.9	0.9	0.0	4.9	4.2	-0.8	42.7	42.8	0.1	51.3	52.0	0.7

Table S9. Percentage of risk areas for each country categorized using PAR values under baseline (BL) and new infrastructure scenarios (BL + NI), with scenario comparison

Country	*Low Risk*			*Moderately Low Risk*			*High Risk*			*Moderately High Risk*			*Highest Risk*		
	BL	**BL+NI**	**Change**	**BL**	**BL+NI**	**Change**	**BL**	**BL+NI**	**Change**	**BL**	**BL+NI**	**Change**	**BL**	**BL+NI**	**Change**
Afghanistan	0.0	0.0	0.0	0.6	0.6	0.0	2.8	2.9	0.1	95.0	94.9	0.0	1.7	1.6	-0.1
Bangladesh	0.0	0.0	0.0	0.0	0.0	0.0	0.0	0.0	0.0	24.9	26.5	1.7	75.1	73.4	-1.7
Bhutan	0.3	0.3	0.0	8.5	7.0	-1.5	17.1	14.1	-3.0	61.0	60.3	-0.7	13.2	18.3	5.1
Brunei Darussalam	20.3	18.5	-1.8	35.9	38.8	2.9	14.4	16.4	2.0	21.0	21.9	0.9	8.4	4.3	-4.0
Cambodia	0.2	0.2	0.0	10.3	10.0	-0.3	12.6	12.5	-0.2	68.0	68.4	0.4	8.9	9.0	0.1
China	0.1	0.1	0.0	4.0	3.4	-0.6	7.7	7.9	0.2	51.8	55.2	3.4	36.5	33.4	-3.0
India	0.7	0.7	0.0	5.2	4.9	-0.3	6.5	6.5	0.0	41.0	43.6	2.6	46.5	44.2	-2.3
Indonesia	1.3	1.1	-0.2	19.8	19.1	-0.7	19.1	19.5	0.4	48.4	50.1	1.8	11.5	10.1	-1.3
Laos	0.3	0.3	0.0	4.9	4.5	-0.4	10.2	10.4	0.1	68.1	69.7	1.6	16.5	15.1	-1.4
Malaysia	3.5	2.6	-0.8	20.6	22.3	1.7	16.4	16.8	0.4	52.3	53.0	0.6	7.2	5.3	-1.9
Myanmar	0.4	0.4	0.0	7.2	6.9	-0.3	7.7	7.8	0.1	64.0	65.2	1.1	20.7	19.8	-0.9
Nepal	0.0	0.0	0.0	1.2	1.3	0.1	3.6	3.9	0.3	40.4	43.4	2.9	54.8	51.4	-3.3
Pakistan	0.0	0.0	0.0	0.3	0.3	0.0	1.2	1.4	0.2	32.7	35.3	2.6	65.8	63.0	-2.8
Papua New Guinea	1.3	1.2	-0.1	41.5	39.8	-1.7	30.3	30.2	-0.2	26.1	28.3	2.3	0.8	0.6	-0.2
Philippines	0.0	0.0	0.0	4.1	3.4	-0.7	8.2	8.2	0.0	61.1	65.6	4.5	26.6	22.8	-3.8
Sri Lanka	0.1	0.1	0.0	0.4	0.8	0.3	1.3	1.9	0.6	16.0	27.1	11.1	82.2	70.1	-12.0
Taiwan	0.1	0.1	0.0	19.6	16.1	-3.5	31.3	37.2	5.8	39.9	42.2	2.3	9.1	4.4	-4.6
Thailand	0.0	0.0	0.0	0.4	0.5	0.0	1.7	1.8	0.0	54.5	56.2	1.7	43.3	41.6	-1.7
Timor-Leste	0.0	0.0	0.0	0.5	0.7	0.1	17.5	20.2	2.7	74.3	74.1	-0.2	7.7	5.0	-2.7
Viet Nam	0.0	0.0	0.0	0.0	0.0	0.0	0.3	0.2	-0.1	23.6	23.4	-0.2	76.0	76.4	0.3

Table S10. Percentage of risk areas for each country categorized using pandemic spread risk values under baseline (BL) and new infrastructure scenarios (BL + NI), with scenario comparison

Country	*Low Risk*			*Moderately Low Risk*			*High Risk*			*Moderately High Risk*			*Highest Risk*		
	BL	**BL+NI**	**Change**	**BL**	**BL+NI**	**Change**	**BL**	**BL+NI**	**Change**	**BL**	**BL+NI**	**Change**	**BL**	**BL+NI**	**Change**
Afghanistan	99.90	99.90	0.00	0.03	0.03	0.00	0.03	0.00	-0.03	0.03	0.07	0.03	0.00	0.00	0.00
Bangladesh	38.31	34.51	-3.79	5.10	4.42	-0.68	26.06	20.77	-5.29	30.35	40.17	9.83	0.19	0.12	-0.06
Bhutan	100.00	100.00	0.00	0.00	0.00	0.00	0.00	0.00	0.00	0.00	0.00	0.00	0.00	0.00	0.00
Brunei Darussalam	100.00	100.00	0.00	0.00	0.00	0.00	0.00	0.00	0.00	0.00	0.00	0.00	0.00	0.00	0.00
Cambodia	99.89	100.00	0.11	0.11	0.00	-0.11	0.00	0.00	0.00	0.00	0.00	0.00	0.00	0.00	0.00
China	97.32	99.38	2.06	1.45	0.22	-1.22	0.98	0.25	-0.73	0.25	0.15	-0.10	0.01	0.01	-0.01
India	88.94	85.63	-3.31	3.51	4.04	0.53	5.54	7.13	1.59	1.98	3.16	1.17	0.03	0.04	0.01
Indonesia	99.88	99.92	0.04	0.01	0.01	0.01	0.06	0.04	-0.02	0.05	0.03	-0.02	0.00	0.00	0.00
Laos	100.00	100.00	0.00	0.00	0.00	0.00	0.00	0.00	0.00	0.00	0.00	0.00	0.00	0.00	0.00
Malaysia	99.82	99.85	0.03	0.00	0.00	0.00	0.09	0.06	-0.03	0.09	0.09	0.00	0.00	0.00	0.00
Myanmar	99.95	99.96	0.01	0.01	0.00	-0.01	0.03	0.00	-0.03	0.01	0.04	0.03	0.00	0.00	0.00
Nepal	99.58	99.42	-0.16	0.00	0.05	0.05	0.21	0.27	0.05	0.16	0.27	0.11	0.05	0.00	-0.05
Pakistan	97.01	95.72	-1.29	1.43	1.48	0.06	1.28	2.44	1.16	0.25	0.32	0.07	0.03	0.03	0.00
Papua New Guinea	100.00	100.00	0.00	0.00	0.00	0.00	0.00	0.00	0.00	0.00	0.00	0.00	0.00	0.00	0.00
Philippines	99.84	99.87	0.03	0.00	0.03	0.03	0.10	0.07	-0.03	0.06	0.03	-0.03	0.00	0.00	0.00
Sri Lanka	100.00	100.00	0.00	0.00	0.00	0.00	0.00	0.00	0.00	0.00	0.00	0.00	0.00	0.00	0.00
Taiwan	100.00	100.00	0.00	0.00	0.00	0.00	0.00	0.00	0.00	0.00	0.00	0.00	0.00	0.00	0.00
Thailand	99.58	99.74	0.16	0.09	0.02	-0.07	0.13	0.07	-0.05	0.18	0.16	-0.02	0.02	0.00	-0.02
Timor-Leste	100.00	100.00	0.00	0.00	0.00	0.00	0.00	0.00	0.00	0.00	0.00	0.00	0.00	0.00	0.00
Viet Nam	98.76	99.55	0.79	0.65	0.20	-0.45	0.37	0.11	-0.25	0.20	0.11	-0.08	0.03	0.03	0.00